Mesoporous silica micro/nanomotors: A new horizon in biomedical applications and precision medicine

Farah M. ElMakaty, Ma.Ellyza Andrea J. Ona, Xiaomin Li, Ahmed A. Elzatahry, Mohamed F. Mady

Applied Materials Today 43 (2025) 102673

Contents lists available at ScienceDirect

Applied Materials Today

journal homepage: www.elsevier.com/locate/apmt

Mesoporous silica micro/nanomotors: A new horizon in biomedical applications and precision medicine

Farah M. ElMakaty [a], Ma.Ellyza Andrea J. Ona [a], Xiaomin Li [b], Ahmed A. Elzatahry [c], Mohamed F. Mady [a,*]

[a] Department of Chemistry and Earth Sciences, College of Arts and Sciences, Qatar University, P.O. Box 2713 Doha, Qatar
[b] Department of Chemistry, State Key Laboratory of Molecular Engineering of Polymers, College of Chemistry and Materials, Fudan University, Shanghai 200433, China
[c] William A. Brookshire Department of Chemical and Biomolecular Engineering, Cullen College of Engineering, University of Houston, Houston, TX 77204, USA

ARTICLE INFO

Keywords:
Nanomotors
Mesoporous silica
Medicine
Structure
Asymmetric

ABSTRACT

Mesoporous silica ($mSiO_2$) micro/nanomotors (MNMs) are a groundbreaking innovation in nanotechnology and versatile tools in biomedical science. Combining active propulsion and advanced functionality, they navigate complex biological environments, overcome the limitations of traditional therapies, and expand the horizons of precision medicine. Central to their versatility is the $mSiO_2$ framework, which offers a high surface area, tunable porosity, and inherent biocompatibility. These properties enable efficient drug loading, controlled release, and functionalization for advanced therapeutic and diagnostic applications. MNMs are designed with diverse structures, including Janus, core-shell, yolk-shell, hollow, and biomimetic architectures, each meticulously tailored to meet the demands of specific biomedical applications. Utilizing active propulsion mechanisms—chemical, light-driven, magnetic, and hybrid—MNMs achieve precise targeting and enhanced efficacy in cancer therapy, cardiovascular treatments, and infection management. This review explores the synthesis methods, structural innovations, and biomedical applications of MNMs, emphasizing their transformative role in overcoming the limitations of passive systems. By leveraging the adaptability of $mSiO_2$, MNMs effectively address critical challenges such as fuel toxicity, hypoxia, dense extracellular matrices, and biofilm resistance. Furthermore, the review highlights future prospects, including the integration of multimodal therapies, optimization of biocompatibility, and expanding clinical applicability, establishing $mSiO_2$-based MNMs as key tools in precision medicine.

1. Introduction

Nanotechnology has emerged as a transformative force in medicine, offering tools and techniques that enable precise interventions at the molecular and cellular levels [1]. This field integrates physics, chemistry, and biology to create nanoscale devices capable of addressing some of the most pressing challenges in modern healthcare. These include enhancing the efficacy of drug delivery systems, improving diagnostic precision, and enabling minimally invasive treatments [2].

In traditional medicine, therapeutic agents often face barriers such as poor bioavailability, nonspecific targeting, and off-target effects, leading to reduced efficacy and undesirable side effects. Nanotechnology addresses these limitations by leveraging structures with tunable properties, such as size, shape, and surface chemistry, to optimize the delivery of therapeutic agents directly to target sites.

Micro/Nanomotors (MNMs), first envisioned by Nobel laureate Richard Feynman in 1959, are nanoscale machines capable of utilizing external stimuli to actively propel through their environment and perform specific tasks [3,4]. By manipulating their components and structure, MNMs can be synthesized to achieve specific functions, making them highly versatile and enabling a wide range of applications, particularly in biomedicine [5].

These MNMs represent a significant advancement in nanotechnology, uniquely converting energy from various sources into mechanical motion. Unlike passive nanoparticles, which are limited by poor penetration through biological barriers and inefficient targeting, MNMs actively navigate biological environments such as blood vessels, tissues, and cellular matrices [6–9]. This active mobility allows them to overcome obstacles, access hard-to-reach sites, and achieve precise therapeutic outcomes. Propulsion mechanisms, including chemical catalysis,

* Corresponding author.
E-mail address: mmady@qu.edu.qa (M.F. Mady).

https://doi.org/10.1016/j.apmt.2025.102673
Received 23 January 2025; Received in revised form 12 February 2025; Accepted 4 March 2025
Available online 13 March 2025

magnetic fields, and light-driven methods, further enhance their capacity for efficient drug delivery and advanced imaging applications.

Among the various types of MNMs, mesoporous silica ($mSiO_2$) MSMs have garnered significant interest due to their structural advantages and functional versatility [10–17]. The high surface area and tunable porosity of $mSiO_2$ allow for efficient drug loading and controlled release, while their biocompatibility ensures minimal adverse effects [18–20]. $mSiO_2$ MSMs combine these features with active propulsion, positioning them as a cornerstone of next-generation biomedical devices. Their development has unlocked new possibilities for targeted drug delivery and cancer therapy [19,21–25], disease treatment [26–28], biofilm eradication [13,29,30], treatment of heavy-metal poisoning [31], real-time diagnostics [32], and combination therapies [33,34], making them highly promising tools for precision medicine [35].

Over the past decade, MNMs have gained attention for their potential applications in biomedicine, particularly in drug delivery, diagnostics, and minimally invasive therapy [36–39]. Several review papers have reported the biomedical applications of MNMs [25,40–44], focusing on targeted drug delivery, diagnostics and imaging, regenerative medicine, and minimally invasive applications [45]. For instance, Zhang et al. [46] provided a comprehensive review of MNMs in cancer therapy and cardiovascular applications, while Dong et al. [47] explored the role of photocatalytic MNMs in drug delivery and environmental applications. Similarly, Tian et al. [2] and Venugopalan et al. [48] examined the advantages of magnetic and intracellular MNMs, respectively.

While previous reviews have explored the biomedical applications of MNMs, our work provides a distinct perspective by integrating synthesis methodologies with biomedical applications, emphasizing how structural design influences functional performance. This review offers a comprehensive analysis of $mSiO_2$-based MNMs, linking synthesis methods, propulsion mechanisms, and material properties to their effectiveness in precision medicine. We highlight the role of tailored synthesis in improving biocompatibility, targeted drug delivery, and multifunctionality while addressing underexplored aspects such as hybrid propulsion systems and clinical translation. By bridging these gaps, this review not only consolidates existing knowledge but also provides a forward-looking perspective on the future of MNMs in biomedical applications.

2. Synthesis methods of biomedical $mSiO_2$ MNMs

The synthesis of biomedical $mSiO_2$ MNMs involves diverse methods that enhance their propulsion, functionality, and adaptability for various applications. Below are key approaches used to fabricate these nanomotors, each providing unique advantages for tasks.

The structural design of $mSiO_2$ MNMs determines their propulsion efficiency, stability, and suitability for specific applications. Various architectures—Janus structures, core-shell designs, yolk-shell frameworks, hollow structures, and membrane-coated biomimetic nanomotors—offer unique advantages that enhance their performance. Each structural type influences the nanomotor's function, motion, and overall effectiveness, tailored to meet the needs of biomedical and environmental applications.

2.1. *Fabrication of $mSiO_2$*

The synthesis of mesoporous silica nanoparticles (MSNs) is achieved through versatile methods, each tailored to specific structural and functional requirements. The sol-gel method is a foundational approach that involves the hydrolysis and condensation of silica precursors like tetraethyl orthosilicate (TEOS) in the presence of surfactants such as cetyltrimethylammonium bromide (CTAB), which guide mesopore formation (Fig. 1a) [49]. Renowned for its simplicity and scalability, this technique serves as the basis for more advanced synthesis strategies. Building on sol-gel chemistry, the Stöber method employs TEOS hydrolysis and condensation in an alcohol-based medium under basic conditions, typically catalyzed by ammonia, to produce monodispersed silica particles. While initially developed for dense silica particles, the introduction of surfactants or block copolymers during synthesis has enabled the creation of mesoporous structures, making it a precise method for applications requiring uniform porous particles (Fig. 1b) [50]. Meanwhile, template-assisted methods utilize templating agents to guide pore formation. Soft templates like CTAB form micelles that structure the silica framework (Fig. 1c), while hard templates such as

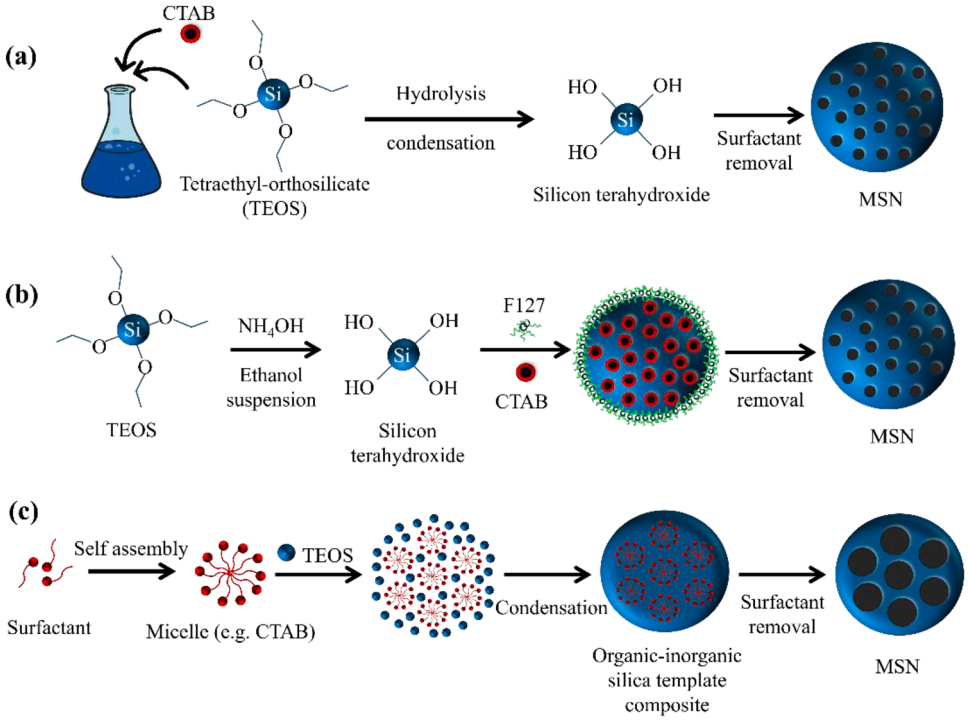

Fig. 1. Schematic representation of different MSN synthesis methods (a) Sol-gel method, (b) modified Stober method, and (c) soft-template assisted method.

nanoparticles or polymer spheres are used to create hollow or hierarchical MSNs by acting as removable core [51]. These approaches emphasize structural precision and high loading capacity.

In addition to these foundational methods, specialized techniques have emerged to achieve unique MSN architectures. One such innovative approach is the bi-phase stratification method, which creates asymmetric MSNs by controlling the distribution of silica precursors across distinct phases during synthesis [52]. This method enables precise manipulation of mesopore orientation and particle morphology, allowing for the design of tailored mesoporous structures optimized for specialized applications such as catalysis, targeted drug delivery, and advanced therapeutic systems. Together, these methods highlight the adaptability and sophistication of MSN synthesis, catering to diverse scientific and industrial needs.

2.2. Building up structures: techniques for structural design and functionalization

Following the synthesis of MSNs, additional structural modifications are crucial to enhance their functionality, propulsion efficiency, and adaptability. The key techniques for building these advanced structures are as follows.

2.2.1. Janus nanomotors: techniques for controlled asymmetry

Janus structures are defined by their asymmetry, with distinct materials on opposite sides enabling complementary functions. This asymmetry disrupts fluid flow, generating directional motion through mechanisms like thermophoresis or bubble generation. Metal-deposited Janus nanomotors achieve this by asymmetrically coating one side of $mSiO_2$ particles with metals, with the choice of metal significantly influencing their behavior.

One widely employed method involves sputtering techniques, where a thin layer of metal, such as gold or platinum, is selectively deposited on one hemisphere of a nanoparticle (Fig. 2a). This approach ensures the anisotropic distribution of functional components and is commonly used to enhance catalytic activity [51,53–58]. Platinum deposition via electron-beam evaporation or sputtering has been demonstrated to achieve precise asymmetric configurations suitable for catalytic propulsion [51,59].

Another approach utilizes wax-emulsion systems, where nanoparticles are embedded in a wax layer to expose only one side for subsequent functionalization or coating. This technique has been used for gold or platinum chemisorption and is effective in generating highly functional Janus structures [52,60,61].

Advanced fabrication strategies include selective growth of secondary materials, such as $mSiO_2$ or organo-silica, on one side of the particle. For instance, $mSiO_2$ shells were grown asymmetrically on upconversion

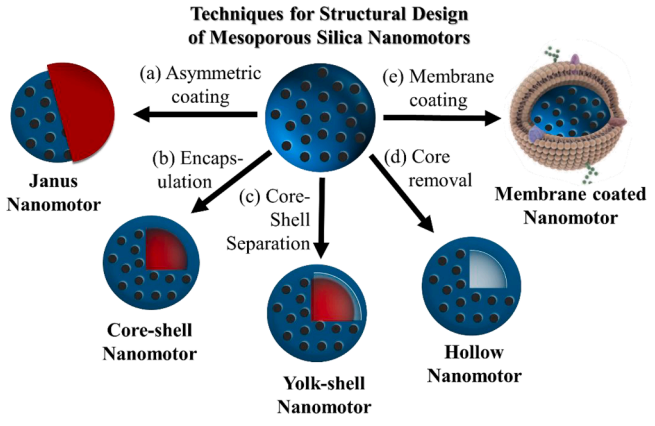

Fig. 2. Structural designs of $mSiO_2$ nanomotors: (a) Janus, (b) hollow, (c) core-shell, (d) yolk-shell, and (e) membrane-coated.

nanoparticles (UCNPs) using a water-oil interface, yielding Janus configurations tailored for imaging and drug delivery applications [62]. Similarly, organo-silica was selectively deposited on gold nanorods or silica-gold nanoparticles to achieve anisotropic functionalization [63,64]. Additionally, thermodynamic-controlled coating has been employed to asymmetrically encapsulate platinum nanoparticles with mesoporous organo-silica, providing robust control over material distribution [65].

2.2.2. Core-shell nanomotors: techniques for functional encapsulation

Core-shell nanomotors consist of a functional core enclosed within a protective shell, providing stability, environmental protection, and controlled cargo release. Advanced synthesis techniques enable precise encapsulation, enhancing structural integrity and functionality. MSNs are commonly used as cores, and coated using techniques such as vesicle fusion with Escherichia coli (E. coli) membranes for a biomimetic shell [66], or gold nano-seed deposition followed by seed growth for a uniform metallic shell [64]. These designs are widely used in drug delivery and imaging due to their biocompatibility and optical properties.

Alternatively, MSNs can form shells around other cores to create multifunctional nanostructures. UCNPs, synthesized via thermal decomposition, are coated with silica using sol-gel methods involving TEOS and surfactants, resulting in nanomotors suitable for photothermal and photodynamic therapies [67,68]. Hydroxyapatite (Hap) cores, produced by calcium carbonate substitution, are coated with $mSiO_2$ using CTAB-TEOS systems, creating acid-responsive carriers ideal for targeted drug release in tumor environments [69].

2.2.3. Yolk-shell nanomotors: technique for controlled core-shell separation

Yolk-shell nanomotors consist of a functional core enclosed within a hollow shell, enabling dynamic core-shell interactions. Tailored with various materials, they enhance propulsion, cargo capacity, and stability for specific applications. One study synthesized yolk-shell structure using a temperature-regulated swelling and asymmetric shrinkage strategy. Polydopamine (PDA) nanospheres were prepared via dopamine polymerization, serving as the yolk. The nanospheres were swollen under controlled reaction temperatures with hexadecyltrimethylammonium chloride (CTAC) surfactant and chlorobenzene, which acted as a swelling agent. A $mSiO_2$ shell was then grown around the swollen PDA core using TEOS as the silica precursor. Upon cooling to room temperature, the PDA core underwent asymmetric shrinkage due to the confinement of the silica shell, resulting in the formation of the yolk-shell structure. This synthesis approach provides precise control over the hollow cavity's size and the yolk-shell architecture, making it a versatile platform for biomedical and nanomotor applications [70].

2.2.4. Hollow nanomotors: techniques for controlled core removal

Hollow nanomotors, composed of a mesoporous shell with an internal cavity, enable a lightweight structure for fast delivery. Hollow nanostructures are synthesized through various strategies that involve the controlled removal of a core material, leaving behind a functional cavity surrounded by a shell. A common method utilizes polystyrene nanoparticles as sacrificial templates. These templates are coated with silica using TEOS via a sol-gel process, followed by core removal through calcination or dissolution in dimethylformamide [56,71–74]. Alternatively, solid silica nanoparticles can serve as templates, with selective etching using sodium carbonate employed to create the hollow structure [75].

Other approaches incorporate metal oxide cores, such as Fe_3O_4, which are removed using hydrochloric acid etching, enabling the formation of $mSiO_2$ shells with unique functionalities [51]. MSNs can also be synthesized directly with surfactant-assisted processes, such as CTAB-TEOS systems, to achieve inherent porosity and hollow configurations. Functionalization with supramolecular host-guest chemistry, such as carboxylatopillar [5]arene, further enhances their utility in modular applications [58]. These methodologies highlight the

adaptability in creating hollow nanostructures tailored for drug delivery, catalysis, and nanomotor applications.

2.2.5. Membrane-coated and biomimetic nanomotors: techniques for functional integration

Membrane-coated biomimetic nanomotors combine synthetic cores with biological membranes to enhance biocompatibility, immune evasion, and targeted delivery. These nanostructures are synthesized using advanced techniques that integrate functional cores with biologically inspired coatings. A common approach involves cloaking nanomotors or nanoparticles with natural membranes, such as macrophage or platelet membranes. For instance, macrophage membranes were used to coat manganese dioxide (MnO_2)-Au-mSiO_2 nanomotors through a coextrusion process, enabling targeted delivery across the blood-brain barrier [53,57]. Similarly, platelet membranes were coated onto mesoporous/macroporous silica-platinum cores via ultrasonic treatment, allowing for thrombus-specific aggregation [76].

Biomimetic structures can also be engineered using bacterial membranes, such as E. coli vesicles, which were fused onto MSNs to create hybrid micromotors with chemotactic behavior [66]. Additionally, macrophage membrane-coated Janus mSiO_2 nanomotors were functionalized with PEG to enhance immunological compatibility and cancer cell targeting [57,63]. Functional modifications, such as the incorporation of DNA probes or enzymes, further expand the applications of these nanostructures. For example, urease-coated nanoparticles decorated with gold and radiolabeled with iodine-124 provided imaging capabilities and catalytic propulsion [50]. These methods illustrate the adaptability of membrane-coated and biomimetic nanostructures, enabling their use in advanced biomedical applications, including targeted therapy, diagnostics, and nanomotor propulsion.

2.2.6. Enzyme conjugation and nanoparticles addition

The integration of enzymes and nanoparticles into mSiO_2 nanomotors requires precise methods to ensure stability, controlled release, and adaptability for diverse biomedical and catalytic applications. Stable covalent attachment techniques, such as 1-ethyl-3-(3-dimethylaminopropyl)carbodiimide (EDC)–N-hydroxysuccinimide (NHS) chemistry, create durable amide bonds, enabling long-term stability, as seen in catalase enzymes used for H_2O_2 decomposition and carboxylated iron oxide nanoparticles facilitating magnetic control [52,72]. Glutaraldehyde is a widely used cross-linking agent that links amine groups on enzymes to the nanomotor surface, creating stable covalent bonds. This method has been used to attach enzymes like urease [77–79], lactate oxidase [80], enhancing biocatalytic performance across various environments. Environmentally responsive attachments, such as disulfide bonds, provide stability in non-reducing conditions but enable targeted release in reductive environments, making them valuable for applications like intracellular magnetic particle delivery [81]. Reversible and dynamic attachment methods, including host-guest chemistry, leverage non-covalent interactions, such as β-cyclodextrin with azobenzene-modified carriers, to allow reversible binding of enzymes and nanoparticles for applications requiring functional flexibility [71]. Electrostatic adsorption, exploiting natural charges between enzymes and nanomotor surfaces, offers non-covalent, reversible binding, enabling precise temporal control over enzyme release or replacement based on environmental conditions [82]. Together, these approaches enable tailored functionality for nanomotors, enhancing their adaptability and efficiency in complex applications.

2.3. Drug loading and delivery

mSiO_2 nanomotors utilize methods such as electrostatic attraction and passive diffusion for effective drug integration and controlled release. Electrostatic Attraction enables drug molecules to be loaded into nanomotors by taking advantage of charge differences between the nanomotor surface and the therapeutic agents. This method is particularly effective for drugs that require controlled release, as the attraction can hold the drugs within the porous structure until environmental changes, such as pH shifts, cause release at targeted locations [81]. Passive Diffusion is another common technique for drug loading in mesoporous nanomotors. In this approach, the drug molecules are absorbed into the nanomotor's porous structure through simple diffusion, driven by concentration gradients. This technique is straightforward and allows for high loading capacity, as drugs gradually diffuse into the large surface area provided by the mesopores. Once loaded, the drugs can be released passively or triggered by stimuli, such as the presence of enzymes or pH changes within cellular environments, ensuring controlled and localized therapeutic effects [59,83].

3. Propulsion mechanisms

Several propulsion mechanisms can be employed by nanomotors. These can utilize either chemical propulsion, light-propulsion, magnetic-propulsion, electric propulsion, or bio-hybrid propulsion mechanisms to convert energy into physical motion in the nanoscale range. Self-propulsion mechanisms including chemical propulsion utilize catalytic reactions such as the urease-mediated breakdown of urea into ammonia and carbon dioxide [69,75], which creates an asymmetric pressure gradient around the nanomotor to drive its motion (Fig. 3a). The catalytic-driven active propulsion of nanomotors is also achieved by functionalization with catalase and glucose oxidase [75]. Light-propelled nanomotors use a light source, such as near infrared (NIR)-irradiation, to stimulate photothermal agents such as gold in Janus nanomotors causing thermophoretic movement, or stimulate the decomposition of a pre-loaded chemical fuel, such as ammonium bicarbonate, to produce carbon dioxide gas for propulsion [56] (Fig. 3b). Magnetically-propelled nanomotors use magnetic fields to propel nanomotors designed to have a magnetic core or an asymmetric magnetic nanoparticle coating [84] (Fig. 3c). Electric-propelled nanomotors utilize electric fields to generate movement by inducing electrophoretic or electroosmotic forces, enabling precise control over their motion at the nanoscale (Fig. 3d). Biohybrid nanomotors which incorporate cellular components into the nanomotor structure are also synthesized to improve its biocompatibility and biodegradability [45].

4. Biomedical applications of mesoporous nanomotors

Nanomotors, with their unique ability to self-propel and actively interact with biological environments, hold immense potential for a wide range of biomedical applications. By leveraging various propulsion methods and incorporating advanced drug-loading and release mechanisms, nanomotors can be engineered to serve as highly efficient drug delivery systems. These innovations enable precise targeting, controlled drug release, and enhanced therapeutic efficacy, making nanomotors promising tools for the treatment and diagnosis of numerous diseases and infections.

4.1. Cancer therapy and tumor penetration

The capability of mesoporous nanomotors to traverse in complex biological environments, release chemotherapeutic drugs specifically to target cells, and be loaded with photodynamic and photothermal agents makes it a suitable platform for the treatment and mitigation of cancer cells. Several studies have focused on improving the efficiency of nanomotors in penetrating tumor cells and interacting with the tumor microenvironment, increasing its efficiency in tumor therapy (Table 1).

4.1.1. Enhanced tumor penetration and accumulation

One of the primary challenges that hinder the effectivity of nanomotor-based cancer treatments is their tumor penetration ability. To address this challenge, enzyme-propelled and NIR-propelled nanomotors have been developed, providing nanomotors with improved

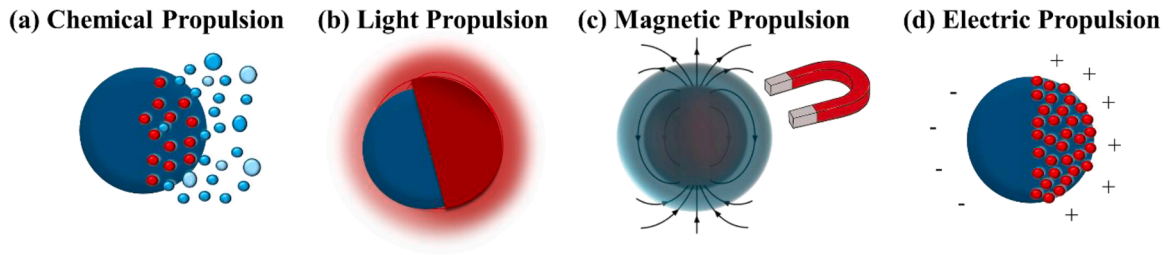

Fig. 3. Propulsion mechanisms of nanomotors: (a) Chemical, (b) Light-driven, (c) Magnetic, and (d) Electric, illustrating various energy sources driving nanoscale motion.

propulsion for deep tumor penetration. Hortelao et al. [79] developed urease-powered MSNs for the delivery of the anticancer drug Doxorubicin (Dox). The synthesized nanomotor, with a solid silica core and urease-functionalized shell, autonomously moves through the decomposition of urea into ammonia and carbon dioxide, improving drug delivery in HeLa cells (Fig. 4a). The results of the MTT assay indicated that the Dox-loaded nanomotors achieved the half maximal inhibitory concentration (IC50) at a 10-times lower concentration compared to passive nanomotors, indicating enhanced drug delivery and tumor penetration due to the nanomotor's self-propulsion and the presence of ammonia as the decomposition by-product. Consequently, Chen et al. [56] synthesized a Janus $mSiO_2$ nanomotor propelled by the NIR-activated decomposition of NH_4HCO_3 to CO_2 and NH_3. The gas-blasting effect produced facilitates endosomal escape and undisrupted Dox release in the tumor cytoplasm. Experiments in blood vessels and tumor-bearing mice models indicated the effective accumulation and penetration of nanomotors in tumor cells. NIR irradiation on the targeted tumor sites increased nanomotor accumulation, leveraging the enhanced penetration and retention effect for improved cancer therapy (Fig. 4b).

Furthermore, the group of Zhang et al. [85] reported the synthesis of rod-shaped Janus nanomotors grafted with urease and hyaluronidase (HAase) for the delivery of Dox towards cancer cells. The Janus nanomotor was synthesized through a seed-defined growth of MSNs on one side of HAp nanorods. While urease acts as a fuel for the nanomotor propulsion, HAase serves as an extracellular matrix (ECM) digesting enzyme, facilitating the longer blood circulation, and enhanced retention and tumor penetration capabilities of the nanomotor.

4.1.2. *Controlled drug release and targeted delivery towards tumor cells*

The ability towards precise targeting of the tumor site, controlled drug release, and biocompatibility are essential considerations when designing nanomotors for drug delivery. Several studies enhance tumor targeting in nanomotors by integrating magnetic-guidance [81], receptor-specific binding [69], and pH-sensitive or enzyme-triggered drug release mechanism [81,86], ensuring the precise and controlled-drug delivery to tumor sites. Li et al. [81] developed magnetic $mSiO_2$ Janus nanomotors for photodynamic therapy (PDT), targeting CCRF-CEM cancer cells. Loaded with methylene blue (MB), reactive oxygen species (ROS) are produced from the nanomotor upon light exposure, facilitating tumor cell apoptosis. The pH-sensitive release of MB, activated by glutathione in the tumor microenvironment minimizes the cell toxicity of the PDT effect. Furthermore, Chen et al. [69] advanced tumor targeting through the synthesis of urease-powered Janus nanomotors modified with hyaluronic acid (HA), a tumor-targeting moiety that binds to CD44 receptors overexpressed in tumor cells. The pH-sensitivity of the Hap core allows the controlled release of Camptothecin in acidic environments, ensuring drug stability. The HA-modified nanomotors indicated an increased cellular internalization in HepG2 cells, confirming its high specificity. Similarly, a pH-responsive boronic-acid gating system on Janus nanomotors is developed by Mayol et al. [86] for the targeted delivery of Dox in HeLa cells. The Iridium-powered nanomotor catalyzes the decomposition of hydrogen peroxide (H_2O_2), facilitating nanomotor propulsion. Glucose oxidase immobilized on the MSN catalyzes the production of gluconic acid, which lowers the pH and triggers the release of Dox in the acidic tumor microenvironment. The performed assays indicated the glucose-dependent, targeted release of Dox, and substantial cancer cell death, confirming the nanomotor's pH-responsive drug delivery mechanism. Hortelao et al. [49] developed urease-powered $mSiO_2$ nanomotors for targeting 3D bladder cancer spheroids through functionalizing the outer surface with urease, polyethylene glycol (PEG) and anti- fibroblast growth factor receptor 3 (FGFR3) antibodies. While PEG enhances the stability and biocompatibility, the anti-FGFR3 antibody allows the nanomotor to target and bind FGFR3, which is overexpressed in bladder cancer cells. The targeting capability of the nanomotor not only enhanced its internalization efficiency, but also inhibited fibroblast growth factor signaling pathways, leading to enhanced cell death in spheroids and reduced tumor proliferation.

4.1.3. *Synergistic cancer therapies*

Nanomotors that integrate different cancer treatment strategies – such as photothermal therapy (PTT), PDT, and chemotherapy, demonstrate enhanced therapeutic efficacy due to the synergistic treatment effects. The previously mentioned study of Chen et al. [56] synthesized a NIR-activated Janus nanomotor loaded with Dox and the photothermal agent PDA, which regulates Dox-release and facilitates the propulsion of the nanomotor through thermophoresis. This combines both chemotherapeutic and PTT strategies to induce the targeted killing of cancer cells. Li et al. [81] enhanced the effect of PDT by designing Pt-catalyzed Janus nanomotors that relieve tumor hypoxia through the decomposition of H_2O_2 to O_2. This boosted oxygen availability and increased the production of ROS, which improved the outcome of PDT on cancer cell apoptosis (Fig. 5a). In addition to hypoxia alleviation, other strategies that employ calcium overload phototherapy along with PDT and PTT have been developed to increase the potency of cancer treatments. Wu et al. [87] designed a CaO_2 and photosensitizer-loaded nanomotor that utilized both chemical and photothermal propulsion to achieve deeper penetration into tumor tissues, and at the same time, promote tumor cell death through the calcium ion-induced mitochondrial membrane potential disruption (Fig. 5b). Another study by Chang at al. [88] reported a nanomotor modified with Ce6 photosensitizer, acyl thioreas (AT), and PEG which can manipulate the tumor microenvironment including oxygen, copper, and ROS levels, alongside PTT and PDT, for the effective inhibition of tumor migration and metastasis, particularly in colorectal cancer. The effect of tumor microenvironments manipulation of the Ce6@AT-PEG-MSN-Pt (CAPMP) nanomotor on tumor treatment was evaluated through *in vitro* experiments wherein it was found that CAPMP nanomotors showed higher cytotoxicity levels compared to the control groups without photosensitizer and Cu chelator due to the synergistic effect of PTT, PDT, hypoxia relief, and Cu depletion (Fig. 5c).

4.2. *Cardiovascular applications*

In recent years, MSNs have emerged as promising therapeutic tools for the treatment of cardiovascular conditions, such as atherosclerosis and vein thrombosis. Through specific modifications and propulsion

Table 1
Nanomotor structures for cancer therapy and tumor penetration.

Structure (**classification**), Size	Schematic illustration	Therapeutic Efficacy (Tumor Penetration)	Mechanistic Benefits	Refs.
$mSiO_2$ partially coated with PDA and loaded with silicon phthalocyanine (**Janus**), 200 nm	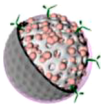	94.6 % apoptosis, reduces tumor cell proliferation to 10.9 %, tumor penetration of 7.53 μm/s		[34]
$mSiO_2$ loaded with pH-responsive catalysts) surrounded by Au nanoparticles (satellite), with Pt nanoparticles partially coating the core (**Janus + core-satellite**), 495 nm	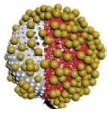		13.5 °C temperature rise under laser, propulsion of 1.26 $\mu m^2/s$	[36]
$mSiO_2$ functionalized with urease and asymmetrically coated with gold nanoparticles (**Membrane-Coated**), 507.8 nm.	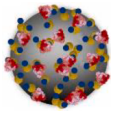	24–38 % penetration in urea and 2–8 % in water		[50]
Hollow $mSiO_2$ loaded with doxorubicin, coated with PDA and ammonium bicarbonate, and asymmetrically covered with gold (**Janus + hollow**), 337 nm	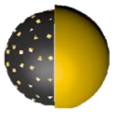		NIR raises temperature by 20.2 °C, over 20 wt. % Dox loading, no damage to healthy tissues observed	[56]
$mSiO_2$ asymmetrically coated with gold, cloaked with macrophage cell membranes (**Janus + Membrane-Coated**), 80 nm	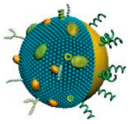	96.2 % cancer cell apoptosis	Propels with a force of 1.3×10^{-14} N	[57]
Platinum- $mSiO_2$ loaded with Dox and capped with redox-sensitive PEG (**Janus**), 100 nm	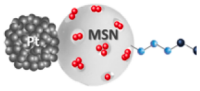		Propels at speeds up to 19.4 μm/s, generates 53 fN propulsion force, 0.7 μmol/g Dox release	[61]
Platinum-mesoporous organosilica functionalized with hyaluronic acid (**Janus**), 256.4 nm	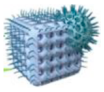		Increases diffusion to 1.49 $\mu m^2/s$ and speed to 2.60 μm/s	[65]
Hydroxyapatite-embedded $mSiO_2$ with an asymmetrically deposited gold layer, functionalized with catalase (**Janus + core-shell**), 86 nm	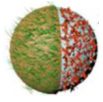	71.4 % tumor reduction, extends survival	Enhances deep penetration, reduces Ki-67-positive tumor cells to 14.7 %	[69]
Hollow $mSiO_2$ asymmetrically coated with silica and functionalized with different enzymes (**Janus + hollow**), 389 nm			Enhances diffusion by up to 83 %, generates a driving force of 64 fN for nanomotor propulsion	[75]
$mSiO_2$ functionalized with urease, loaded with Dox (**core-shell**), 344 nm		Improves drug uptake over 24 h	Boosts drug release by 4x, reduces cancer cell viability with 10x fewer nanobots	[79]
PEGylated gold-coated dendritic $mSiO_2$ loaded with ferrous sulfide, lonidamine, and lactate oxidase (**Janus**), 102 nm		Tumor penetration of 5.44 μm/s	increases diffusion coefficient to 0.93 $\mu m^2/s$ in acidic environments	[80]
Magnetic silica cores asymmetrically coated with Pt nanoparticles, loaded with MB (**Janus**), 120–159 nm		Kills 96 % cancer cells, spares 70 % normal cells	Boosts oxygen by 32 %, drug release 85.5 %, low hemolysis of 1.71 %	[81]
$mSiO_2$ loaded with a dye or doxorubicin, functionalized with benzimidazole, and capped with cyclodextrin-modified urease (**core-shell**), 418 nm	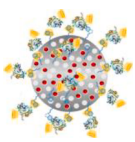	Cell viability reduced by 28 %	Boosts drug release to 40 % at acidic pH	[83]

(*continued on next page*)

Table 1 (*continued*)

Structure (**classification**), Size	Schematic illustration	Therapeutic Efficacy (Tumor Penetration)	Mechanistic Benefits	Refs.
Iridium- $mSiO_2$ loaded with Dox and gated with glucose oxidase for pH-sensitive release (**Janus**), 109 nm	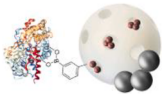	Induces 83–85 % HeLa cell death	Boosts diffusion to 9.8 $\mu m^2/s$, high drug loading, releases 89 μg/mL drug in 3 h	[86]
CaO_2-loaded MSNs with photosensitizer, 460 nm	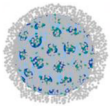	79.5 % apoptosis	Enhances CD8+ T cells by 2.6-fold, shrinks tumors to 18.4 mm^3	[87]
Pt- $mSiO_2$ with copper chelator and photosensitizer (**Janus**), 150–200 nm	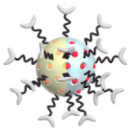	Reduces tumor growth by 90 %, 80 % survival rate	Boosts ROS, reverses hypoxia, inhibits metastasis	[88]
$mSiO_2$ asymmetrically coated with platinum and chromium, loaded with Dox (**Janus**), 75 nm	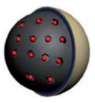		Achieves a speed of 20.2 μm/s, generates a propulsion force of 13.47 fN.	[89]

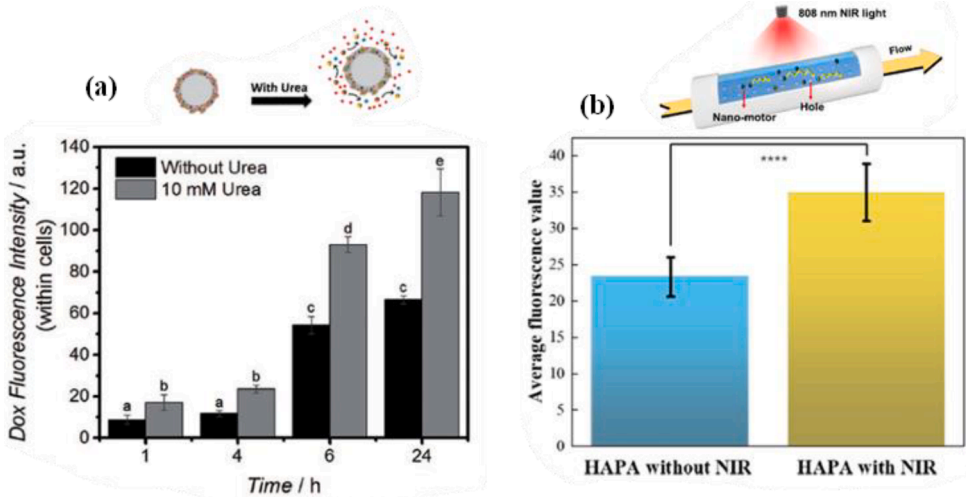

Fig. 4. Enhanced penetration of $mSiO_2$ nanomotors. (a) Intracellular fluorescence analysis of core-shell $mSiO_2$ functionalized with urease demonstrates improved Dox uptake by enzyme-powered nanobots in the presence of urea, highlighting motion-assisted drug delivery [79], and (b) Quantification of fluorescence intensity in porous membranes shows increased penetration of hollow $mSiO_2$ nanomotors asymmetrically covered with gold, demonstrating NIR-driven self-propulsion [56].

mechanisms, MSNs have demonstrated remarkable potential in overcoming the limitations of traditional treatment strategies, including enhanced drug targeting, bioavailability, and therapeutic outcomes in cardiovascular diseases (Table 2) [51,62,76,90].

4.2.1. *Atherosclerosis treatment*

Atherosclerosis, characterized by the gradual narrowing of arteries due to plaque formation, presents significant challenges in treatment. Recent advancements in MSN-based therapies have demonstrated their potential to address these challenges. For example, Zhang et al. [62] developed an NIR-propelled Janus upconversion nanomotor (UCNP@$mSiO_2$) for atherosclerosis amelioration, which releases nitric oxide (NO) upon NIR irradiation (980 nm) for effective endothelial penetration and plaque reduction. The NIR-triggered NO-propulsion mechanism of the nanomotor prevents its adherence toward the endothelial cell lining in the blood vessels and Reticuloendothelial System (RES) capture, increasing the nanomotor's bioavailability. At the same time, the produced NO also alleviated the plaque formation as shown through *in vivo* models, proving the potential of the nanomotor for the treatment of atherosclerosis. Likewise, Huang et al. [91] also reported platelet-derived NIR-propelled Janus $mSiO_2$ nanomotors loaded with paclitaxel (PTX) and anti-VCAM-1 antibody for atherosclerosis combination therapy. The asymmetric coating of the $mSiO_2$ nanomotor with Pt allows for NIR-propulsion and photothermal therapy, combining the effects of the sustained release of PTX and the NIR-induced heat for the eradication of inflammatory macrophages. Furthermore, its biomimetic targeting capabilities due to the platelet membrane coating ensures targeted drug delivery, enhances the nanomotor circulation time, and prevents premature PTX release.

4.2.2. *Thrombosis management*

Thrombosis, caused by blood clots that obstruct veins or arteries, represents another critical cardiovascular condition. MSN-based nanomotors have shown great promise in thrombolysis by leveraging their unique structural and functional features. Tao et al. [90] developed bowl-shaped $mSiO_2$ nanomotors designed for targeted thrombolysis (Fig. 6a), utilizing NO not only as a propellant but also as a therapeutic agent for reducing oxidative stress, and enhancing clot dissolution. The

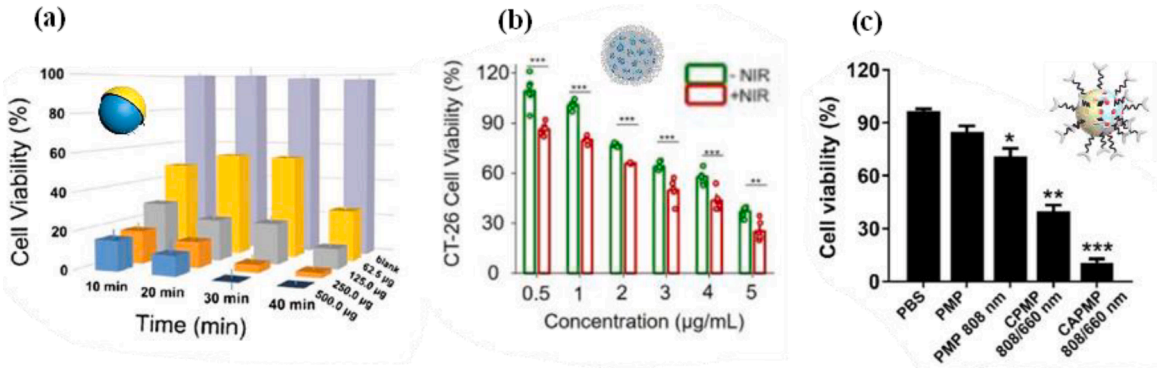

Fig. 5. Nanomotor-assisted PDT enhances selective cancer cell killing. (a) Viability of CCRF-CEM cells decreases with increasing concertation of Janus Pt-coated nanomotors and irradiation time, confirming enhanced PDT cytotoxicity [81]. (b) *In vitro* antitumor activity of CaO_2-loaded nanomotor against CT-26 cells shows significantly lower viability under NIR irradiation, demonstrating phototherapy synergy [87]. (c) LoVo cell viability analysis after incubated with various formulas reveals that combining tumor microenvironment modulation with PDT achieves the most potent cancer cell inhibition. PBS (control) shows high viability, while PMP (Platinum-Modified Particles) with 808 nm laser demonstrates PTT CPMP (PMP + Chlorin e6) under 808/660 nm laser shows enhanced photothermal and PDT. CAPMP (complete formulation) under 808/660 nm achieves the lowest viability due to synergistic PTT, PDT, and oxygen generation [88].

Table 2
Nanomotor structures for cardiovascular applications.

Structure (**classification**), Size	Schematic illustration	Therapeutic Efficacy	Mechanistic Benefits and Biocompatibility	Refs.
Hollow $mSiO_2$ loaded with heparin (**Janus + hollow**), 200 nm		Improves anticoagulant properties.	Moves at 40–212 μm/s, shows 0.58 % hemolysis rate.	[51]
UCNPs with $mSiO_2$ coatings loaded with Roussin's Black Salt (**Janus + Membrane-Coated**), 120 nm		Reduces plaque areas significantly ($P < 0.01$).	Retains 85.57 % nanomotors in blood flow, increases nanoparticle transmittance in vessels, maintains normal liver and kidney function markers	[62]
Platelet coated with porous silica and loaded with Dox (**Membrane coated**), 410 nm		Reduces thrombus volume to <5 % in 7 days	Penetrates thrombus up to 4000 μm with NIR, retains 26 % nanomotors at thrombus site, shows no organ toxicity.	[76]
Bowl-shaped $mSiO_2$ loaded with NO donor, 225 nm		Boosts fibrinolysis to 74 %, reducing fibrin area to 17 %, cuts thrombus volume to 0.20 after 7 days	Moves at ~3.5 μm/s in plasma and endothelial cells, shows <2 % hemolysis and no toxicity.	[90]
Heparin-loaded tubular mesopores composed of poly(3,4-ethylenedioxythiophene), $mSiO_2$, and manganese dioxide, 6 μm		heparin release under catalytic conditions resulted in a 322.1 μg release over 12 h	Moves at 23 μm/s, shows 5 % hemolysis rate and low nanomotor cytotoxicity	[92]

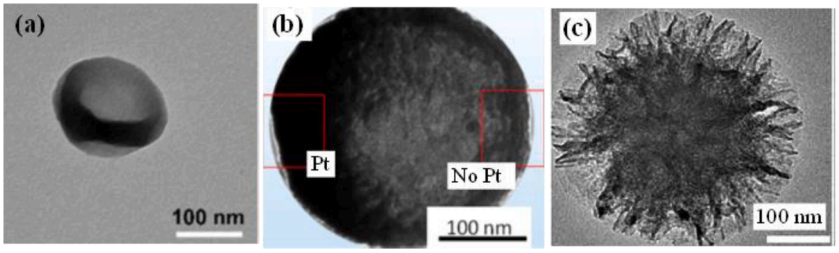

Fig. 6. TEM characterization of nanomotors for thrombosis treatment. (a) bowl-shaped NO-driven nanomotors, facilitating NO-driven motion for enhanced thrombus targeting and dissolution [90]. (b) Janus heparin-loaded nanomotors illustrate structural asymmetry, enabling sequential thrombolysis and anticoagulation [51]. (c) Platelet-derived porous nanomotors confirms platelet membrane coating and Pt nanoparticle distribution for biomimetic targeting [76].

mesopores of the nanomotor are loaded with two therapeutic agents, L-Arginine which reacts with excessive ROS to produce NO, and Urokinase (UK), which dissolves the thrombus. While the ROS-triggered NO release improves the mobility of the nanomotor, it also provides a sustained drug availability at the thrombolytic site, while promoting the endothelialization process, making the thrombolytic treatment more effective.

In addition to this, the challenge of sustained anticoagulant delivery

and prevention of thrombi reformation is equally crucial in thrombus management. In response to the need for long term anticoagulation, Hu et al. [51] designed a Pt-propelled Janus heparin-loaded nanomotor tailored for sustained anticoagulant release (Fig. 6b). The evaluation of the drug-release performance of the heparin-loaded nanomotor indicated a higher drug release quantity and a longer release time that lasts for 25 days compared to its non-hollow counterpart, indicating the contribution of its high adsorption capacity to its sustained drug release. The study provided a platform that not only enhances the bioavailability and targeting of the drug but also prevents clot reformation after thrombolysis. While [90] and [51] reported the improved drug delivery and retention of nanomotors, challenges on precise thrombus targeting and achieving deep penetration into the clot still remain. To address these challenges, Wan et al. [76] designed a platelet-derived mesoporous/macroporous silica nanomotor for biomimetic targeting with NIR-propulsion capabilities for a more enhanced penetration depth

Table 3
Nanomotor structures for infection treatment and antibacterial applications.

Structure (**classification**), Size	Schematic illustration	Antibacterial and Therapeutic Efficacy	Performance and Biocompatibility	Refs.
$mSiO_2$ head with MnO_2 tentacles, encapsulated in macrophage membranes, and coated with gold (**Janus + Membrane-Coated**), <100		Scavenges ROS with 64.6 % efficiency, increases M2/M1 microglia ratio to 2.6	No organ toxicity	[53]
$mSiO_2$ asymmetrically coated with gold and loaded with near-infrared photosensitizers (**Janus**), 306 nm		Reduces biofilm biomass by 71 % in 3 min	Moves at 86.1 μm/s, no adverse effects	[55]
Dendritic $mSiO_2$ doped with manganese dioxide, loaded with NO donors, and asymmetrically coated with gold nanoparticles (**Janus**), 80 nm	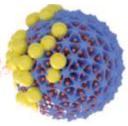	Cuts bacterial load by 4 orders, penetrates biofilms to 7.1 μm, heals wounds by 93.2 % in 9 days	99.9 % antibiofilm efficiency, no toxicity	[60]
Neutrophils loaded with MSNs and coated with gold (**core-shell + membrane coated**) 88 mm	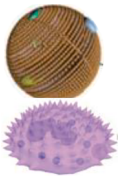	Targets infection sites and delivers drugs efficiently	97.36 % nanoparticle uptake, 80 % cell viability, moves at 0.165 μm/s, pH response drug release with minimal leakage	[66]
Hollow $mSiO_2$ loaded with magnetic nanoparticles and photosensitizers, and functionalized with catalase (**hollow**), 2 um with a hole of 400 nm	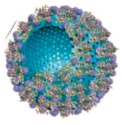	Kills 72.5 % E. coli	Produces 20 % more singlet oxygen, no toxicity	[72]
$mSiO_2$ doped with magnesium and zinc nanoparticles, functionalized with urease (**Core-satellite**), 695 nm	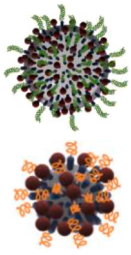	Cuts bacterial load by 3 orders	Diffusion 0.73 $\mu m^2/s$, shows no toxicity in mice	[77]
$mSiO_2$ functionalized with urease, lysozyme, and catalase, and coated with gold, 411 nm	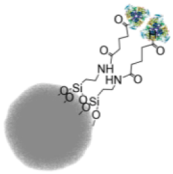	Reduces biofilm by 60 %, kills 82 % E. coli	Diffusion 0.87 $\mu m^2/s$, no toxicity observed	[78]
Cerium dioxide-doped $mSiO_2$ coated with Au (**Janus**), 190 nm	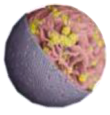	boosts antibacterial effects by penetrating biofilms, reduces inflammation by scavenging ROS	Temperature rises to 59.15 °C, no toxicity	[93]
$mSiO_2$ asymmetrically coated with Au and loaded with photosensitizers (**Janus**), 120 nm	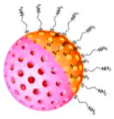	Kills >99.5 % bacteria in 10 min, achieves 80 % death in 7 min	High biocompatibility, targets bacteria at pH 4.6	[94]

(Fig. 6c). The design of the nanomotor incorporates both thrombolytic and anticoagulant drugs, UK and heparin, through a sequential drug release system, providing an all-encompassing approach for clot dissolution and prevention, significantly enhancing the effect of thrombolytic treatments.

Furthermore, addressing the challenge of uncontrolled drug release and poor retention at target sites, Wang et al. [92] synthesized catalytically-propelled mesoporous tubular micromotors loaded with heparin. This micromotor has an inner layer of MnO_2 for catalytic propulsion, a $mSiO_2$ middle layer which provides a high surface area for drug loading, and an outer layer of Poly(3,4-ethylenedioxythiophene) which provides structural integrity to the micromotor. The sustained heparin release from the nanomotor was reported to be consistent for over six days under static conditions, with a higher rate under active conditions, enhancing the therapeutic efficiency of the micromotor.

4.2.3. *Heavy metal poisoning treatments*

Beyond cardiovascular applications, MSNs have also been explored for the treatment of heavy metal poisoning. Liu et al. [31] synthesized magnetically propelled Silica/ε-Polylysine nanomotors for the removal of Pb^{2+} in blood, achieving high biocompatibility, low cytotoxicity, and high Pb^{2+} removal efficiency compared to passive adsorbents. Furthermore, the magnetic properties of the nanomotor not only enhanced the contact probability with hemoglobin-bound Pb^{2+}, but also allows for nanomotor recovery and reuse.

4.3. *Infection treatment and antibacterial applications*

Bacterial infections, especially those associated with biofilms and antibiotic resistance, remain a major global health challenge [55,60,78]. However, the treatment of bacterial infections through antibiotics often fall short due to issues such as the rise of multi-drug resistant bacteria, off-target effects, and poor drug penetration into biofilms. To address these limitations, current research has focused on the development of nanomotors that can resolve a range of infection-related challenges, such as the eradication of biofilm, enhanced drug delivery, and the use of PTT and PDT. This section highlights studies that developed significant advances in the use of $mSiO_2$-based nanomotors to improve the efficiency of nanomotor-based bacterial treatments (Table 3).

4.3.1. *Biofilm penetration and eradication*

The poor penetration in biofilms is one of the key challenges that hinder the efficiency of nanomotors in antibacterial applications. A study by Zheng et al. [60] addressed the challenge of low penetration ability of conventional drug treatments on biofilms through designing self-propelled dendritic $mSiO_2$ nanomotors (AG-DMSNs) driven by the active production of NO through a cascade catalytic reaction. Using methicillin-resistant *Staphylococcus aureus* (MRSA) biofilm as a model, it was confirmed that the Janus nanomotor achieves enhanced biofilm penetration and can efficiently reduce the colony-forming units within the biofilm by 99.9 %, demonstrating the potential of AG-DMSNs for the treatment of antibacterial infections (Fig. 7a). While Zheng et al. [55] explored the use of NO-propelled nanomotors to improve biofilm penetration, the group of Maric et al. advanced this concept by designing thermophoretic $mSiO_2$-Au nanomotors powered by NIR light. The light-driven propulsion allows the precise control of the nanomotor, wherein increasing the power of the applied NIR laser increases the velocity of the nanomotors. The ultra-fast movement exhibited by the nanomotor increased the efficiency of the nanomotor's biofilm penetration and eradication performance, which was proven through eradication and penetration assays performed with *P. aeruginosa* biofilms. Building upon the NIR-driven thermophoretic propulsion mechanism demonstrated by [55], Bai et al. [93] improved nanomotor design by designing Janus nanomotors with cerium-doped mesoporous silica (CeM) and gold nanoparticle coating, enhancing biofilm penetration and eradication for periodontitis treatment. With its active motion and photothermal capabilities, the nanomotor has the ability to overcome the physical barriers of biofilms and disrupt bacterial cells, reducing the bacterial load in biofilms. *In vitro* tests suggested that the NIR-powered Janus nanomotors (J-CeM@Au) demonstrated enhanced biofilm penetration abilities, attributed to the photothermal damage induced by the nanomotor on the biofilm (Fig. 7b). The presence of CeO_2 nanoparticles also enables the nanomotor to scavenge the excess ROS in the periodontal microenvironment, reducing inflammation and promoting tissue regeneration.

4.3.2. *Targeted antibacterial action in systemic infections*

Recent studies on enhancing the effectiveness of nanomotor-based antibacterial treatment have introduced advancements that allow for a

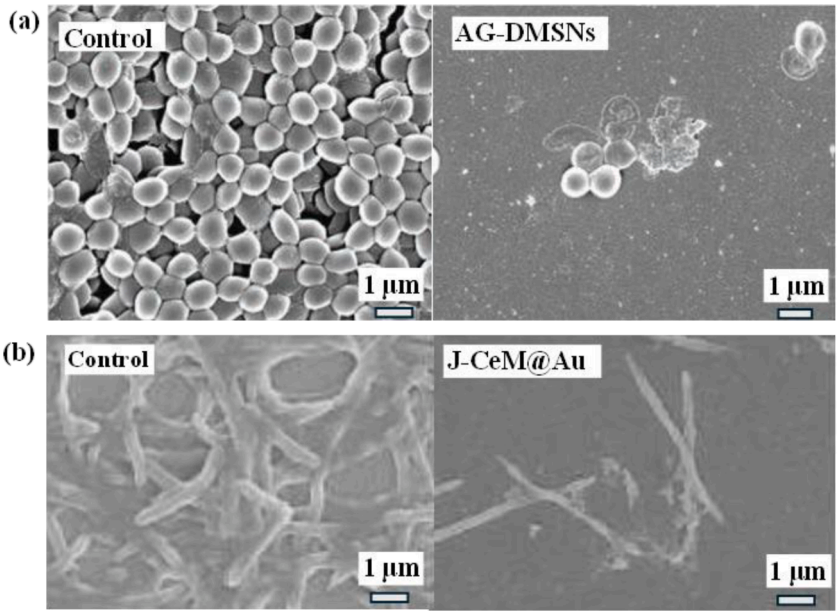

Fig. 7. SEM images showing biofilm eradication after nanomotor treatments. (a) Biofilm of MRSA before and after treatment with AG-DMSNs, demonstrating significant biofilm disruption due to NO-driven motion [60]. (b) Biofilm before and after treatment with J-CeM@Au nanomotors, highlighting effective biofilm eradication through NIR-driven ROS scavenging [93].

more accurate bacteria targeting to minimize the treatment's off-target effects.

Arque et al. [77] synthesized urease-powered $mSiO_2$ based MNMs that are designed to deliver antimicrobial peptide payloads (LL-37 and K7-Pol) toward the target infection site. The study highlighted the use of nanomotors for the treatment of systemic infections, particularly through using *Acinetobacter baumannii* abcesses in a mouse model. *In vitro* tests confirmed that the antimicrobial nanomotors exhibited bactericidal effects against both Gram-positive and Gram-negative bacteria, while *in-vivo* anti-infective activity tests suggested that the MNMs have the ability to exert their antibacterial effects not only at the administered site, but throughout the infected tissue, overcoming the limitations of conventional passive treatments. Similarly, Vilela et al. [78] also synthesized urease-powered mesoporous $mSiO_2$ nanomotors (U-MSNPs) for the treatment of urinary tract infections caused by *E. coli*. Their findings suggested the efficiency of the urease-functionalized nanomotors in disintegrating *E. coli* biofilms at a concentration of 200 μg/mL, proving their potential for the treatment of infectious diseases. These suggest that the self-propulsion and targeting capabilities of nanomotors can be leveraged to address challenges related to systemic side effects that are typically observed with passive drug delivery methods.

4.3.3. *Non-antibiotic therapies: photothermal and photodynamic therapies*

Previous studies have developed NIR-propelled nanomotors for tackling biofilm-associated infections, which focused primarily on the penetration of biofilms to facilitate the eradication of bacteria. However, while biofilm penetration is crucial for treating chronic infections associated with biofilms, it is equally important to consider the next step of bacterial lysis, which effectively kills the bacteria after it has been exposed. Loukanov et al. [94] developed NIR-powered Janus nanomotors for the targeted photothermal lysis of bacteria such as *E. coli*. In his work, the gold-coated Janus nanomotors were able to induce cellular damage on bacterial cells through the localized heat produced upon NIR irradiation. The generation of localized heat through surface plasmon resonance disrupts the bacterial cell membranes, facilitating rapid cell death. In addition, functionalizing the Janus nanomotor with cysteamine allows it to specifically target *E. coli* through electrostatic

Table 4
Nanomotor structures for diagnostics and imaging applications.

Structure (**classification**), Size	Schematic illustration	Diagnostic and Imaging Performance	Mechanistic Benefits	Refs.
$mSiO_2$ asymmetrically functionalized by DNA onto one face, while catalase is immobilized on the other face (**Janus**), 500 nm MSN particles	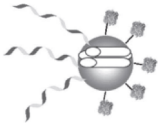	Detects DNA with 3.2x hybridization efficiency	Transports DNA-functionalized cargo using hybridization with 50–57 % DNA grafting	[52]
$mSiO_2$ functionalized with catalase and loaded with fluorescent and magnetic imaging agents (**Janus +hollow**) 390 ± 12 nm.		Diffusion speed increased 8.36 × in fluorescence imaging	Boosts diffusion to 0.96 $\mu m^2/s$, maintains 85 % cell viability	[58]
AuNR-PMO functionalized with periodic mesoporous organosilica and gold nanorods (**Janus**), 50 nm	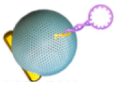	Captures 86.12 % miRNA, detects miRNA at 12.22x improvement	Elevates temperature to 57.8 °C for detection	[63]
Upconversion nanomotors with a $mSiO_2$ core, gold shell coating, loaded with near-infrared responsive dyes (**core-shell**), 130 nm	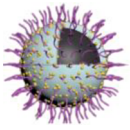	Strong red UCL signal at 659 nm for nanomotor tracking	Moves at 3.86 μm/s under NIR, penetrates tumors up to 100 μm, no toxicity or organ damage observed	[67]
$mSiO_2$ asymmetrically coated with platinum and gold, functionalized with catalase, and loaded with photosensitizers (**Janus + core-shell**), 60 nm	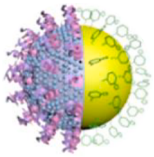	Tumor fluorescence and photoacoustic signals increased post-injection	Boosts diffusion to 2.11 $\mu m^2/s$, reduces tumor volume by 90.3 % in, no toxicity or organ damage observed	[68]
Enzyme-powered $mSiO_2$ functionalized with catalase and equipped with pH-responsive DNA nanoswitches (**hollow**), 2 um	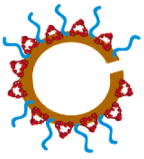	Tracks pH changes via FRET nanoswitch	Moves at 6.4 μm/s in 100 mM urea, shows 123 s activity half-life, no adverse effects observed	[74]
Gadolinium-doped $mSiO_2$ with Au (**Janus**), 70 nm	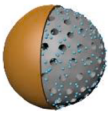	Achieves 4.8x brighter MR signals	Propels at 3.49 $\mu m^2/s$ under NIR, shows 90 % cell viability and no toxicity	[95]
Janus Au-NR@$mSiO_2$ with a $mSiO_2$ coating, functionalized with therapeutic agents (**Janus**), 109 nm		Imaging contrast improved by 65 % with ultrasound	Velocity of 0.73 μm/s with ultrasound, ensures 100 % survival with no toxicity	[96]

interactions, making the treatment targeted. Consequently, the study of Xu et al. utilized urease-propelled micromotors capable of PDT for the treatment of *E. coli* infections. Functionalized with the photosensitizer, 5,10,15,20-tetrakis(4-aminophenyl)porphyrin (TAPP), the micromotor generates singlet oxygen ($^1O_2$) which causes oxidative damage to bacterial cell membranes, leading to bacterial death [72]. The study reported an increased singlet oxygen generation and a greater bactericidal effect against *E. coli* for the urease-driven micromotors compared to stationary micromotors, suggesting a more enhanced PDT effect. These studies demonstrate the potential of MNMs capable of PTT and PDT towards antibacterial applications.

4.4. Diagnostics and imaging

Several studies have explored the applications of nanomotors in diagnostic and imaging. These multifunctional nanomotors that combine enhanced imaging capabilities and synergistic therapy address multiple key challenges including poor tumor penetration and limited imaging sensitivity (Table 4).

Conventional diagnostic imaging techniques, though effective, are often hindered by limited tissue penetration, poor resolution in dense tissues, and insufficient targeting of deep-seated tumors. This is addressed by incorporating the active propulsion mechanisms of nanomotors to navigate deep-seated tumor regions, improving the accumulation of contrast agents, and thereby enhancing the imaging resolution and sensitivity of diagnostic tools.

The study of Zheng et al. [95] designed NIR-propelled Janus Gd-doped mSiO_2 nanomotors for enhanced Magnetic Resonance (MR) imaging. The mSiO_2 core provides a high surface area for doping with gadolinium, which serves as the contrast agent for MR imaging. The MR images obtained for 4T1 cancer cells incubated with JMS nanomotors under NIR radiation indicated an increased MR signal intensity, confirming its enhanced cellular uptake and improved imaging contrast *in vitro* (Fig. 8a). Furthermore, *In vivo* studies indicated an improved accumulation in tumor tissues and a significant increase in MR signal when nanomotors are subjected to NIR irradiation, allowing for deep-tissue imaging. These results are attributed to the active motion of nanomotors through NIR irradiation which directly enhances tumor penetration, accumulation, and MR imaging. Similarly, a study by Ye et al. [96] developed US-propelled Janus mSiO_2 nanomotors loaded with 2,2-azobis[2-(2-imidazolin-2-yl) propane] dihydrochloride (AIPH) (Au-NR-mSiO_2/AIPH) for deep tumor NIR-II photoacoustic imaging combined with ultrasound (US) imaging. The results from *in vivo* tests followed by US/photoacoustic imaging suggested the accumulation of nanomotors and an enhanced imaging contrast in tumor tissues. While the US-propulsion capabilities of the nanomotors allowed the visualization of deep-seated tumors, it also demonstrated an effective anticancer effect through combined sonodynamic and gas therapy.

Chen et al. [68] built on this concept of combined therapy, imaging, and diagnostics through designing a dual-source powered nanomotor capable of dual-modal imaging (fluorescence imaging and photoacoustic imaging), Surface-Enhanced Raman Scattering (SERS) sensing for tumor marker detection, and synergistic PDT and PTT. Dual modal imaging allows the visualization of nanomotors in the tumor sites (Fig. 8b), while the SERS functionality allows the real-time detection of H_2O_2 levels, a biomarker associated with tumor cells. Incorporating PTT and PDT capabilities in the nanomotor contributes to its enhanced anti-tumor effect, facilitated by the alleviation of tumor hypoxia. The multifunctional nanomotor provides a single platform that integrates precise diagnostics, high-resolution imaging, and synergistic therapy which enhances the effectiveness of cancer diagnosis and treatment. Similarly, Liu et al. [67] developed an NIR-driven UCNPs@m-SiO_2-Au-Cys nanomotor for tumor multimode imaging and PTT/PDT. This nanomotor allows for fluorescence and infrared thermal imaging due to the upconversion luminescence of the UNCP core and the photothermal imaging signals provided by AuNPs under NIR irradiation. Strong UCL signals were detected upon NIR exposure (980 nm) of the nanomotors with MCF-7 cells, which clearly visualized the distribution of the nanomotors in the cytoplasm. Furthermore, the photothermal conversion of the nanomotors were evaluated through infrared thermal imaging, which indicated an enhanced thermal effect from the nanomotors in the tumor region upon NIR irradiation (Fig. 8c). The nanomotor's fluorescence and infrared thermal imaging capabilities for its *in-vivo* monitoring provides a comprehensive platform for tumor theranostics.

The biomedical applications of mesoporous nanomotors, as discussed in the previous section, are inherently linked to their structural and functional design. The effectiveness of these nanomotors in targeted drug delivery, diagnostics, and therapy is dictated by key parameters such as size, propulsion mechanisms, and surface modifications. Therefore, the following section delves into the fundamental design trends that influence nanomotor performance, highlighting how structural innovations contribute to their biomedical utility.

5. Trends in nanomotor design: understanding structural impact on performance

Advancements in nanomotor design have revealed critical trends that underscore the impact of structural innovations on performance and therapeutic efficacy. By comparing various architectures such as Janus, core-shell, yolk-shell, hollow, and biomimetic designs, clear relationships emerge between specific structural features and their functional outcomes. As summarized in Table 5, these structures exhibit distinct advantages based on their design: Janus structures with

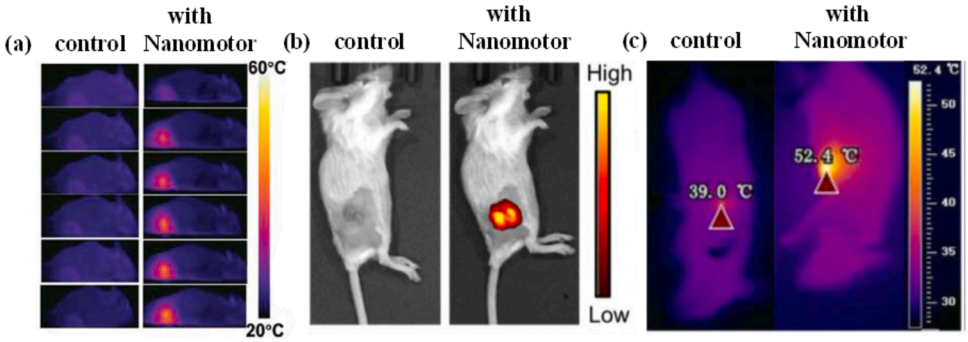

Fig. 8. *In vivo* imaging and synergistic therapy of tumor-bearing mice. (a) Thermal imaging of 4T1 tumor-bearing mice after treatment with Janus Gd-doped nanomotors under NIR irradiation (808 nm), showing temperature elevation over 30 min, indicating effective photothermal conversion [95].
(b) Fluorescence imaging of 4T1 tumors before and after injection with core-shell asymmetrically coated with platinum and gold nanomotors, highlighting significant accumulation at tumor sites for enhanced imaging [68]. (c) IRT images of mice injected with UCNPs@mSiO_2-Au-Cys nanomotors and exposed to 808 nm NIR, demonstrating localized temperature rise and photothermal therapy efficiency [67].

Table 5
Comparative features of advanced nanomotor structures.

Feature	Janus Structures	Core-Shell Structures	Yolk-Shell Structures	Hollow Structures	Membrane-Coated and Biomimetic Nanomotors
Design	Two distinct materials on opposite hemispheres	Core enclosed by continuous shell	Movable or semi-detached core inside a hollow shell	Fully hollow structure with a porous shell	Biological membrane coating
Key Structural Purpose	Dual functionality (e.g., imaging and propulsion); for applications requiring multifunctionality.	Stabilizes core material and enables controlled release; ideal for protecting sensitive materials over time.	Movable core enhances responsiveness to stimuli; suited for smart drug delivery or photothermal therapy.	Fully hollow and porous for reduced drag; optimal for fast targeted delivery or environmental remediation.	Ensures biocompatibility and immune evasion; ideal for targeted delivery in biological systems.
Cargo Capacity	Limited due to asymmetric design	Limited to space within the shell	High internal cargo space	Limited to space within the shell	Moderate capacity within the membrane-coated shell
Advantages	Efficient propulsion and multifunctionality	Enhanced stability and controlled release	Large internal volume and adaptive motion	Reduced drag with fast motion	Biocompatibility with immune system evasion
Challenges	Limited cargo space	Constrained adaptability	Complex fabrication, core movement may reduce stability	Limited stability, complex loading	Limited functional customization
Refs.	[34,51,52,54–65,68,69,73,75,80,81,86,88,89,93–103]	[61,64,66,68,69,79]	[55,70]	[51,56,58,71–75]	[26,50,52,53,57,63,66,76,99]

asymmetric compositions enable enhanced propulsion and multifunctionality, while core-shell and hollow designs focus on controlled release and increased cargo capacity. Biomimetic coatings further enhance biocompatibility and immune evasion, making them particularly effective in dense biological environments. The trends across therapeutic, antibacterial, diagnostic, and imaging applications further emphasize how tailored nanomotor designs optimize size, speed, and efficacy to address specific biomedical challenges within each domain.

5.1. Size trends

Nanomotor sizes vary widely, reflecting their application-specific requirements. For therapeutic applications, sizes range from 70 nm to 6 μm (6000 nm), with smaller designs (<500 nm) suited for rapid targeting and interaction with biological environments, while larger nanomotors (>2 μm) focus on sustained effects, such as extended drug release. In antibacterial applications, sizes span 80 nm to 2 μm (2000 nm). Smaller designs (<200 nm) effectively penetrate biofilms and enhance bacterial eradication, while larger systems prioritize payload delivery and multifunctionality for treating complex infections. Diagnostic and imaging applications demonstrate a similar pattern, with nanomotors ranging from 50 nm to 2 μm. Smaller structures excel in molecular diagnostics, such as miRNA detection and DNA hybridization, whereas larger designs support complex monitoring tasks like pH tracking using FRET nanoswitches.

5.2. Speed trends

Speed is critical for active propulsion and dynamic applications. In therapeutic nanomotors, speeds range from 0.165 μm/s to 212 μm/s, with faster designs (>40 μm/s) facilitating rapid drug delivery and navigation in fluid environments, and slower speeds supporting localized and sustained therapeutic effects. Antibacterial nanomotors display speeds between 0.165 μm/s and 86.1 μm/s, where higher speeds improve biofilm penetration and disruption, while slower designs enable sustained antibacterial activity. Diagnostic and imaging applications feature speeds from 0.73 μm/s to 6.4 μm/s. Moderate speeds (2–4 μm/s) balance imaging precision with nanomotor tracking, while higher speeds enable real-time diagnostics, such as dynamic pH monitoring.

5.3. Efficacy trends

5.3.1. Therapeutic applications

The efficacy of therapeutic nanomotors is influenced by their structural design and responsiveness to specific targets. Janus structures excel in rapid targeting and drug delivery due to their asymmetric compositions, which enhance mobility and precision. These nanomotors are highly effective for localized interventions, such as thrombus reduction, achieving therapeutic outcomes like reducing clot volumes by over 95 %. Larger designs, such as core-shell and hollow nanomotors, prioritize sustained drug delivery, exemplified by systems releasing 322.1 μg of heparin over 12 h. The inclusion of catalytic elements and environmentally responsive materials (e.g., pH-sensitive coatings) further enhances therapeutic precision and adaptability to physiological conditions.

5.3.2. Cardiovascular applications

In cardiovascular applications, efficacy is determined by a balance of speed, targeting, and sustained action. Smaller Janus structures excel in rapid thrombus targeting and localized drug delivery, achieving thrombus volume reductions of over 95 %. Larger systems, such as core-shell and hollow designs, focus on sustained anticoagulant therapy, exemplified by prolonged heparin release over 12 h. Biomimetic coatings enhance immune evasion, improving circulation time and effectiveness in dynamic vascular environments. Structural adaptability allows these nanomotors to function efficiently in both acute interventions and long-term management, such as plaque prevention and thrombus resolution.

5.3.3. Antibacterial applications

In antibacterial applications, efficacy trends are shaped by the ability of nanomotors to penetrate biofilms and eradicate pathogens. Smaller, faster nanomotors, such as Janus structures, effectively disrupt biofilms, reducing biomass by 60–71 % within minutes, and reduce bacterial loads by 3–4 orders of magnitude. Larger, multifunctional systems, like hollow and biomimetic designs, sustain antibacterial effects, achieving eradication rates of 72.5–99.5 % for pathogens such as E. coli. Structural elements like ROS scavenging functionalities and antibacterial agent integration enhance their effectiveness, particularly against biofilm-forming bacteria. Biomimetic coatings improve immune evasion and allow nanomotors to function effectively in challenging biological environments.

5.3.4. Diagnostic and imaging applications

Diagnostic and imaging applications prioritize molecular detection and signal amplification, with efficacy driven by structural versatility. Janus nanomotors provide enhanced precision for detecting molecular markers, achieving miRNA capture rates of 86.12 % and sensitivity improvements of 12.22 ×. Core-shell designs enhance imaging stability and contrast, while hollow nanomotors support dynamic monitoring, such as pH tracking via FRET nanoswitches. Multifunctionality is a

critical trend, with nanomotors combining fluorescence, photoacoustic, and MR imaging modalities to improve diagnostic accuracy. Integration of catalytic or upconversion materials ensures robust signal enhancement, exemplified by MR signal brightness increases of 4.8 × .

5.4. General observations

The overall performance of nanomotors reflects careful balancing of size, speed, and efficacy. Smaller nanomotors (<200 nm) prioritize speed and targeting, excelling in applications requiring real-time functionality, such as imaging and diagnostics. Larger designs (>1 μm) focus on payload capacity and sustained effects, making them ideal for therapeutic applications. High speeds (>20 μm/s) are essential for active navigation and dynamic diagnostics, while moderate speeds (2–10 μm/s) support multifunctional applications. Across all applications, efficacy is enhanced by integrating targeted mechanisms such as ROS scavenging, fluorescence imaging, and biofilm penetration, which improve therapeutic and diagnostic precision

6. Challenges in nanomotor development

6.1. Fuel toxicity and biocompatibility concerns

The development of biocompatible propulsion mechanisms is essential to ensure the safety of nanomotors in biomedical applications. The use of toxic propulsion agents, such as H_2O_2 and heavy metals, contribute to harmful cellular oxidative stress and imposes cell toxicity issues [68,79]. Although H_2O_2 is an effective fuel source for propulsion, it generates ROS that can damage healthy tissues and cells [51,60,76]. Likewise, incorporating metallic catalysts such as manganese or platinum raises concerns on the potential systemic toxicity and long-term biocompatibility of the nanomotor [51,76].

6.2. Navigating biological barriers

Tumor environments with dense extracellular matrices and hypoxia is one of the factors that impede the efficacy of imaging and therapeutic agents [67,96]. ECM is a structure composed of proteins and polysaccharides that provide support to cells. Unlike normal cells, the ECM in tumor cells becomes abnormally dense, limiting the penetration and cellular uptake of nanoparticles and drugs [56,79,95]. Furthermore, while ROS production demonstrated a significant therapeutic potential in cancer treatment, the hypoxic tumor microenvironment presents a critical challenge by limiting ROS generation during PDT [87], This limitation not only diminishes treatment efficacy but can also enhance tumor cell invasiveness, increasing the risk of metastasis [88]. Addressing this challenge requires strategies such as oxygen-generating nanomotors or combination therapies that alleviate hypoxia and simultaneously boost ROS production.

Despite advancements such as NO-releasing and NIR light-driven nanomotors, effectively navigating dense bacterial biofilms, particularly for multi-drug-resistant strains remains a significant challenge [55,60,78]. Additionally, the use of certain components, such as metal ions (e.g., Mn^{2+}, Cu^{2+}) and byproducts like ROS or hydrogen peroxide (H_2O_2), can pose toxicity risks to normal tissues [55,60,93]. As such, further innovation is needed to enhance penetration and sustained antibacterial efficacy while minimizing adverse effects.

6.3. Drug delivery efficiency and drug bioavailability

Enhancing the bioavailability, retention at target sites, and tumor-selectivity of nanomotors remains a concern for the delivery of therapeutic agents for cancer treatment and cardiovascular applications. *In vivo*, nanomotors often face systemic clearance by the RES, reducing their effective concentration at tumors and target tissues [68,95]. In addition, their interaction with plasma proteins and immune cells increases the off-target accumulation of nanomotors. While proven to be effective, light- and chemically- propelled nanomotors may have limited retention particularly in dynamic biological environments like the blood stream. The efficacy of thrombolytic drugs, for example, is diminished due to the limited drug retention at thrombus sites affected by rapid blood flow [90].

6.4. Therapeutic synergy

Several challenges are presented by the integration of multimodal therapies, such as PTT, PDT and imaging for nanomotor-based cancer treatment [67,68,96]. The combination of various therapeutic strategies imposes challenges due to the distinct operational requirements needed for each approach. PDT and PTT, for example, often rely on different wavelengths. In addition, traditional photosensitizers, require activation from visible or UV light, which has poor tissue penetration capabilities and can damage healthy cells. This constraint imposes challenges for the treatment of deep-seated tumors. Similarly, US and laser light-propelled nanomotors commonly used for theranostic applications may impose damage towards surrounding healthy cells, requiring their stimuli to be precisely controlled to minimize damage and systemic toxicity.

7. Conclusion and future prospects

MNMs have assumed a pivotal role in revolutionizing biomedicine, offering capabilities that exceed the performance of traditional therapeutic and diagnostic tools. Their propulsion mechanisms – including catalytic, light-driven (e.g. NIR, UV), magnetic, and ultrasonic methods – enable precise targeting of tumors and tissues, overcoming biological barriers such as deep-seated tumors and dense bacterial biofilms. By combining active motion with high biocompatibility and structural versatility, MNMs improve drug delivery efficiency and diagnostic imaging, positioning them as a cornerstone in personalized and precision medicine.

Recent advances in nanomotor synthesis have led to diverse structural designs, including Janus, core-shell, yolk-shell, hollow, and biomimetic architectures, each tailored for specific biomedical applications. Different fabrication techniques such as sol-gel processing, template-assisted fabrication, physical vapor deposition, surface functionalization, and bioconjugation have further enabled precise control over propulsion, drug loading, and release kinetics. In drug delivery, enzyme-powered and light-driven nanomotors have demonstrated superior tumor penetration, precise targeting, and controlled release, significantly improving cancer therapy outcomes. Magnetic and biomimetic nanomotors have also shown promise in cardiovascular treatments by enhancing drug bioavailability and sustaining therapeutic effects. For infection treatment, NIR-driven nanomotors have improved biofilm penetration and bacterial eradication, providing innovative solutions against antibiotic-resistant infections. Additionally, catalytic and US-driven nanomotors have advanced theranostic applications through the integration of tumor penetration and contrast agent delivery with high-resolution imaging.

Despite these achievements, several limitations hinder the potential of nanomotors for bio-applications. Toxicity concerns remain for some propulsion fuels (e.g. H_2O_2) and catalytic metals, posing risks for biocompatibility issues. The effective penetration of nanomotors through biological barriers, such as dense extracellular matrices in tumors and resilient bacterial biofilms, continues to impede the efficiency of its therapeutic and diagnostic applications. The limited bioavailability of therapeutic agents due to the nanomotors interaction with plasma proteins and clearance by the RES also hinders the potency of nanomotor-based treatment strategies. Furthermore, the integration of multimodal treatment strategies in nanomotors also poses challenges, particularly in meeting the specific operational requirements of each therapeutic mode. As such, future efforts in this field should focus on the following:

Use of Biocompatible Fuels and Hybrid Propulsion Mechanisms. The development of enzyme-powered nanomotors that primarily uses biocompatible substrates such as glucose, triglycerides, and urea, would reduce the risks of toxicity issues. Combining the use of these biofuels with light or US-driven propulsion provides a promising solution, improving the safety of the nanomotor design while maintaining its efficient movement. This approach provides greater control in dynamic biological environments, and at the same time ensures its safe use for sensitive systems such as the bloodstream.

Oxygen-generating and Enzymatic Nanomotors for ECM Degradation. To be able to navigate complex tumor microenvironments, nanomotors can be designed to carry ECM-degrading enzymes such as collagenase or hyaluronidase, enabling the localized breakdown of the matrix. The degradation of the ECM would allow the nanomotors to deeply penetrate within the tumor tissues, improving the delivery of therapeutic agents in hypoxic tumor tissues. Furthermore, addressing the hypoxia in tumors through incorporating catalase or manganese oxide (MnO) in nanomotors would improve the efficiency of PDT. Through these strategies, the penetration and therapeutic efficiency in nanomotors in tumors would be significantly enhanced.

Nitric-Oxide (NO)-Releasing Nanomotors for Biofilm Eradication. NO is a potent molecule that has the capability of dispersing biofilms through activating phosphodiesterases, which in turn degrade cyclic-di-GMP molecules critical for biofilm integrity [60]. The incorporation of NO-releasing nanomotors into self-propelled nanomotors offers a promising strategy to enhance biofilm penetration and improve the exposure of bacteria to antimicrobial agents. Furthermore, the combination of NO-release with the mechanical disruption of biofilm layers through the motility of nanomotors could significantly boost antibacterial efficacy. However, the role of NO in inducing ROS must be managed to mitigate its potential damage to host tissues. Given this, future research should focus on controlled, localized NO release, integrating ROS-scavenging agents to mitigate damage, and precise targeting to minimize off-target effects. These advancements will ensure the safety and efficacy of NO-releasing nanomotors for antibacterial therapy.

Improved Light-Responsive Nanomotor Design. To meet the specific operational requirements of combined PTT and PDT strategies, the development of nanomotors with dual-function photosensitizers (e.g. UNCPs) is imperative. This approach overcomes the limitations of UV and visible light, enabling the simultaneous activation of PTT and PDT.

To conclude, mesoporous silica MNMs represent a transformative technology, offering potential towards overcoming challenges in drug delivery, infection treatment, and cancer theranostics. While there have been significant developments in the field, the focus must shift toward addressing limitations by prioritizing biocompatibility, enhancing biological barrier penetration, and seamlessly integrating multimodal strategies. These advancements in nanomotor design will pave the way for more effective and safer nanomotors, reshaping its capabilities for combating cancer and complex diseases.

CRediT authorship contribution statement

Farah M. ElMakaty: Writing – original draft, Validation, Software, Methodology, Formal analysis, Data curation. **Ma.Ellyza Andrea J. Ona:** Writing – original draft, Software, Investigation, Formal analysis, Data curation. **Xiaomin Li:** Writing – review & editing, Supervision. **Ahmed A. Elzatahry:** Supervision, Resources, Project administration, Funding acquisition, Conceptualization. **Mohamed F. Mady:** Writing – review & editing, Validation, Supervision, Software, Resources, Project administration, Investigation, Funding acquisition, Conceptualization.

Declaration of competing interest

The authors declare that they have no known competing financial interests or personal relationships that could have appeared to influence the work reported in this paper.

Acknowledgments

This work was supported by Grant no. ARG01–0602–230467 from Qatar National Research Fund (a member of the Qatar Foundation). The statements made herein are solely the responsibility of the authors. Open access publication of this article is funded by the Qatar National Library.

Data availability

No data was used for the research described in the article.

References

[1] C. Liu, C. Tian, J. Guo, X. Zhang, L. Wu, L. Zhu, B. Du, Research progress of metal–Organic frameworks as drug delivery systems, ACS Appl. Mater. Interfaces 16 (33) (2024) 43156–43170.
[2] J. Tian, N. Gao, M. Wang, M. Zhou, G. Ling, P. Zhang, Application of magnetic micro/nanomotors in biomedicine, ACS Appl. Nano Mater. 7 (6) (2024) 5745–5760.
[3] H. Huang, S. Yang, Y. Ying, X. Chen, J. Puigmartí-Luis, L. Zhang, S. Pané, 3D Motion manipulation for micro- and nanomachines: progress and future directions, Adv. Mater. 36 (1) (2024) 2305925.
[4] A. Elnaggar, S. Kang, M. Tian, B. Han, M. Keshavarz, State of the art in actuation of micro/nanorobots for biomedical applications, Small Sci. 4 (3) (2024) 2300211.
[5] N. Murali, S.B. Das, S. Yadav, S.K. Rainu, N. Singh, S. Betal, Advanced biomimetic and biohybrid magnetic micro/nano-machines, Adv. Mater. Technol. 9 (19) (2024) 2400239.
[6] X. Xia, Y. Li, X. Xiao, Z. Zhang, C. Mao, T. Li, M. Wan, Chemotactic micro/nanomotors for biomedical applications, Small 20 (6) (2024) 2306191.
[7] J. Fu, D. An, Y. Song, C. Wang, M. Qiu, H. Zhang, Janus nanoparticles for cellular delivery chemotherapy: recent advances and challenges, Coord. Chem. Rev. 422 (2020) 213467.
[8] Z. Rahiminezhad, A.M. Tamaddon, S. Borandeh, S.S. Abolmaali, Janus nanoparticles: new generation of multifunctional nanocarriers in drug delivery, bioimaging and theranostics, Appl. Mater. Today 18 (2020) 100513.
[9] X. Zhang, Q. Fu, H. Duan, J. Song, H. Yang, Janus nanoparticles: from fabrication to (Bio)applications, ACS Nano 15 (4) (2021) 6147–6191.
[10] A. Gupta, A.M. Choudhury, J. Meena, S. Bauri, P. Maiti, Ordered mesoporous silica delivering siRNA as cancer nanotherapeutics: A comprehensive review, ACS Biomater. Sci. Eng. 10 (5) (2024) 2636–2658.
[11] X. Li, S. Wang, X. Wang, Y. Luan, D. Wang, X. Du, Dual-propelled polydopamine@SiO2@Pt micromotor with asymmetrical yolk-mesoporous shell for the enhanced catalytic reduction, Mater. Today Chem. 35 (2024) 101916.
[12] D. Vilela, A.C. Hortelao, R. Balderas-Xicohténcatl, M. Hirscher, K. Hahn, X. Ma, S. Sánchez, Facile fabrication of mesoporous silica micro-jets with multi-functionalities, Nanoscale 9 (37) (2017) 13990–13997.
[13] M. Žiemytė, A. Escudero, P. Díez, M.D. Ferrer, J.R. Murguía, V. Martí-Centelles, A. Mira, R. Martínez-Máñez, Ficin–Cyclodextrin-based docking nanoarchitectonics of self-propelled nanomotors for bacterial biofilm eradication, Chem. Mater. 35 (11) (2023) 4412–4426.
[14] L. Kong, C. Chen, F. Mou, Y. Feng, M. You, Y. Yin, J. Guan, Magnesium particles coated with mesoporous nanoshells as sustainable therapeutic-hydrogen suppliers to scavenge continuously generated hydroxyl radicals in long term, Part. Part. Syst. Charact. 36 (2) (2019) 1800424.
[15] Q. Wang, T. Li, D. Fang, X. Li, L. Fang, X. Wang, C. Mao, F. Wang, M. Wan, Micromotor for removal/detection of blood copper ion, Microchem. J. 158 (2020) 105125.
[16] W. Lv, S. Shao, J. Zhang, J. Li, Y. Huang, C. Mao, Preparation of Fe3O4/SiO2@CDS@Pt micromotors for dual-mode detection of blood lead, ChemistrySelect 8 (25) (2023) e202301650.
[17] M. Yan, D. Ma, B. Qiu, T. Liu, L. Xie, J. Zeng, K. Liang, H. Xin, Z. Lian, L. Jiang, B. Kong, Superassembled hierarchical asymmetric magnetic mesoporous nanorobots driven by smart confined catalytic degradation, Chem. A Eur. J. 28 (29) (2022) e202200307.
[18] X. Ma, H. Feng, C. Liang, X. Liu, F. Zeng, Y. Wang, Mesoporous silica as micro/nano-carrier: from passive to active cargo delivery, a mini review, J. Mater. Sci. Technol. 33 (10) (2017) 1067–1074.
[19] M. Vafaeezadeh, W.R. Thiel, Periodic mesoporous organosilica nanomaterials with unconventional structures and properties, Chem. A Eur. J. 29 (33) (2023) e202204005.
[20] L. Zhao, Y. Zhang, Y. Yang, C. Yu, Silica-based nanoparticles for enzyme immobilization and delivery, Chem. Asian J. 17 (17) (2022) e202200573.
[21] J. Feng, J. Zou, X. Li, X. Du, Biomimetic submicromotor with NIR light triggered motion and cargo release inspired by cuttlefish, Nanoscale 15 (41) (2023) 16687–16696.

[22] F. Tong, J. Liu, L. Luo, L. Qiao, J. Wu, G. Wu, Q. Mei, pH/ROS-responsive propelled nanomotors for the active treatment of renal injury, Nanoscale 15 (14) (2023) 6745–6758.

[23] L. Mei, Q. Ding, Y. Xie, H. Liu, H. Li, E. Kim, X. Shen, Y. Zhang, S. Zhang, J.S. Kim, Self-propelling intelligent nanomotor: A dual-action photothermal and starvation strategy for targeted deep tumor destruction, Biomaterials 315 (2025).

[24] M.S. El-Okaily, A.M.A. El-Seidy, E.H. Ismail, R.M. Allam, A.A. Saeed, A. Bhaumik, A.A. Mostafa, Nanoarchitectonics of catalytic tubular nanomotors based on Cu/Fe@SBA-15 for lung cancer treatment, J. Mater. Res. 39 (12) (2024) 1741–1757.

[25] Q. Zhou, Y. Kong, X. Zhou, L. Ren, H. Jiang, D. Lou, J. Xiao, R. Bian, Navigating therapeutic opportunities and challenges with micro/nanomotors in Translational medicine: A review, ACS Appl. Nano Mater. 7 (20) (2024) 23321–23336.

[26] L. Wang, A.C. Hortelão, X. Huang, S. Sánchez, Lipase-powered mesoporous silica nanomotors for triglyceride degradation, Angew. Chem. Int. Ed. 58 (24) (2019) 7992–7996.

[27] J. Han, J. Ye, J. Shi, Y. Fan, X. Yuan, R. Li, G. Niu, M. Abubakar, Y. Kang, X. Ji, A programmable oral nanomotor microcapsule for the treatment of inflammatory bowel disease, Adv. Funct. Mater. (2024).

[28] P. Díez, B. Esteban-Fernández de Ávila, D.E. Ramírez-Herrera, R. Villalonga, J. Wang, Biomedical nanomotors: efficient glucose-mediated insulin release, Nanoscale 9 (38) (2017) 14307–14311.

[29] L. Liu, S. Li, K. Yang, Z. Chen, Q. Li, L. Zheng, Z. Wu, X. Zhang, L. Su, Y. Wu, J. Song, Drug-free antimicrobial nanomotor for precise treatment of multidrug-resistant bacterial infections, Nano Lett. 23 (9) (2023) 3929–3938.

[30] Z. Luo, R. Wang, X. Deng, T. Chen, X. Ma, Y. Zhang, C. Gao, A. Wu, Janus mesoporous organosilica/platinum nanomotors for active treatment of suppurative otitis media, Nanoscale 16 (6) (2024) 3006–3010.

[31] Z. Liu, T. Xu, M. Wang, C. Mao, B. Chi, Magnetic mesoporous silica/ε-polylysine nanomotor-based removers of blood Pb2+, J. Mater. Chem. B 8 (48) (2020) 11055–11062.

[32] J. Grzelak, J. Gázquez, A. Grayston, M. Teles, F. Herranz, N. Roher, A. Rosell, A. Roig, M. Gich, Magnetic mesoporous silica nanorods loaded with ceria and functionalized with fluorophores for multimodal imaging, ACS Appl. Nano Mater. 5 (2) (2022) 2113–2125.

[33] Y. Zhang, Y. Xing, H. Zhou, E. Ma, W. Xu, X. Zhang, C. Jiang, S. Ye, Y. Deng, H. Wang, J. Li, S. Zheng, NIR-activated Janus nanomotors with promoted tumor permeability for synergistic photo-immunotherapy, Acta Biomater. 190 (2024) 463–475.

[34] Z. Zhang, T. Xia, P. Ran, J. Wei, J. Meng, G. Zhang, X. Li, Persistent luminescence-activated Janus nanomotors with integration of photodynamic and photothermal cancer therapies, Chem. Eng. J. 457 (2023) 141226.

[35] Y. Yu, L. Liang, T. Sun, H. Lu, P. Yang, J. Li, Q. Pang, J. Zeng, P. Shi, J. Li, Y. Lu, Micro/nanomotor-driven intelligent targeted delivery systems: dynamics sources and frontier applications, Adv. Healthc. Mater. 13 (27) (2024) 2400163.

[36] Y. Xing, M. Zhou, T. Xu, S. Tang, Y. Fu, X. Du, L. Su, Y. Wen, X. Zhang, T. Ma, Core@satellite Janus nanomotors with pH-responsive multi-phoretic propulsion, Angew. Chem. Int. Ed. Engl. 59 (34) (2020) 14368–14372.

[37] J. Fu, J. Jiao, W. Ban, Y. Kong, Z. Gu, H. Song, X. Huang, Y. Yang, C. Yu, Large scale synthesis of self-assembled shuttlecock-shaped silica nanoparticles with minimized drag as advanced catalytic nanomotors, Chem. Eng. J. 417 (2021) 127971.

[38] M. Kneidinger, A. Iturmendi, C. Ulbricht, T. Truglas, H. Groiss, I. Teasdale, Y. Salinas, Mesoporous silica micromotors with a reversible temperature regulated on–Off polyphosphazene switch, Macromol. Rapid Commun. 40 (22) (2019) 1900328.

[39] X. Ma, X. Wang, K. Hahn, S. Sánchez, Motion control of Urea-powered biocompatible hollow microcapsules, ACS Nano 10 (3) (2016) 3597–3605.

[40] M. Yan, K. Liang, D. Zhao, B. Kong, Core-shell structured micro-nanomotors: construction, shell functionalization, applications, and perspectives, Small 18 (3) (2022) 2102887.

[41] D. Wang, A. Mukhtar, M. Humayun, K. Wu, Z. Du, S. Wang, Y. Zhang, A critical review on Nanowire-motors: design, mechanism and applications, Chem. Rec. 22 (8) (2022) e202200016.

[42] X. Chen, C. Zhou, W. Wang, Colloidal motors 101: A beginner's guide to Colloidal motor research, Chem. Asian J. 14 (14) (2019) 2388–2405.

[43] T. Zhao, X. Li, On the approach to nanoscale robots: understanding the relationship between nanomotor's architecture and active motion, Adv. Intell. Syst. 5 (7) (2023) 2200429.

[44] J. Feng, X. Li, T. Xu, X. Zhang, X. Du, Photothermal-driven micro/nanomotors: from structural design to potential applications, Acta Biomater. 173 (2024) 1–35.

[45] M. Yan, L. Xie, J. Tang, K. Liang, Y. Mei, B. Kong, Recent advances in heterosilica-based micro/nanomotors: designs, biomedical applications, and future perspectives, Chem. Mater. 33 (9) (2021) 3022–3046.

[46] H. Zhang, J. Tang, H. Cao, C. Wang, C. Shen, J. Liu, Review of the applications of micro/nanorobots in biomedicine, ACS Appl. Nano Mater. 7 (15) (2024) 17151–17192.

[47] R. Dong, Y. Cai, Y. Yang, W. Gao, B. Ren, Photocatalytic micro/nanomotors: from construction to applications, Acc. Chem. Res. 51 (9) (2018) 1940–1947.

[48] P.L. Venugopalan, B. Esteban-Fernández de Ávila, M. Pal, A. Ghosh, J. Wang, Fantastic voyage of nanomotors into the cell, ACS Nano 14 (8) (2020) 9423–9439.

[49] A.C. Hortelão, R. Carrascosa, N. Murillo-Cremaes, T. Patiño, S. Sánchez, Targeting 3D bladder cancer spheroids with urease-powered nanomotors, ACS. Nano 13 (1) (2019) 429–439.

[50] A.C. Hortelao, C. Simó, M. Guix, S. Guallar-Garrido, E. Julián, D. Vilela, L. Rejc, P. Ramos-Cabrer, U. Cossío, V. Gómez-Vallejo, T. Patiño, J. Llop, S. Sánchez, Swarming behavior and *in vivo* monitoring of enzymatic nanomotors within the bladder, Sci. Robot. 6 (52) (2021).

[51] S. Hu, S. Shao, H. Chen, J. Sun, J. Zhai, H. Zheng, M. Wan, Y. Liu, C. Mao, J. Zhao, Preparation and properties of Janus Heparin-loaded ammoniated-hollow mesoporous silica nanomotors, J. Phys. Chem. C 122 (17) (2018) 9680–9687.

[52] J. Simmchen, A. Baeza, D. Ruiz, M.J. Esplandiu, M. Vallet-Regí, Asymmetric hybrid silica nanomotors for capture and cargo transport: towards a novel motion-based DNA sensor, Small 8 (13) (2012) 2053–2059.

[53] J. Ye, Y. Fan, Y. She, J. Shi, Y. Yang, X. Yuan, R. Li, J. Han, L. Liu, Y. Kang, X. Ji, Biomimetic self-propelled asymmetric nanomotors for cascade-targeted treatment of neurological inflammation, advanced science (Weinheim, Baden-Wurttemberg, Germany) 11(22) (2024) e2310211.

[54] M. Xuan, Z. Wu, J. Shao, L. Dai, T. Si, Q. He, Near infrared light-powered Janus mesoporous silica nanoparticle motors, J. Am. Chem. Soc. 138 (20) (2016) 6492–6497.

[55] T. Maric, A. Løvind, Z. Zhang, J. Geng, A. Boisen, Near-infrared light-driven mesoporous SiO2/Au nanomotors for eradication of Pseudomonas aeruginosa biofilm, Adv. Healthc. Mater. 12 (13) (2023) 2203018.

[56] W. Chen, R. Jiang, X. Sun, S. Chen, X. Liu, M. Fu, X. Yan, X. Ma, Self-fueled Janus nanomotors as active drug carriers for propulsion behavior-reinforced permeability and accumulation at the tumor site, Chem. Mater. 34 (16) (2022) 7543–7552.

[57] M. Xuan, J. Shao, C. Gao, W. Wang, L. Dai, Q. He, Self-propelled nanomotors for thermomechanically percolating cell membranes, Angew. Chem. Int. Ed. Engl. 57 (38) (2018) 12463–12467.

[58] Z. Ye, Y. Che, D. Dai, D. Jin, Y. Yang, X. Yan, X. Ma, Supramolecular modular assembly of imaging-trackable enzymatic nanomotors, Angew. Chem. Int. Ed. 63 (16) (2024) e202401209.

[59] X. Ma, K. Hahn, S. Sanchez, Catalytic mesoporous janus nanomotors for active cargo delivery, J. Am. Chem. Soc. 137 (15) (2015) 4976–4979.

[60] J. Zheng, W. Wang, X. Gao, S. Zhao, W. Chen, J. Li, Y.N. Liu, Cascade catalytically released nitric oxide-driven nanomotor with enhanced penetration for antibiofilm, Small 18 (52) (2022) 2205252.

[61] P. Díez, E. Lucena-Sánchez, A. Escudero, A. Llopis-Lorente, R. Villalonga, R. Martínez-Máñez, Ultrafast directional janus Pt–Mesoporous silica nanomotors for smart drug delivery, ACS Nano 15 (3) (2021) 4467–4480.

[62] Y. Zhang, C. Liao, M. Abudusaimaiti, H. Zhou, J. Liu, W. Li, Y. Zhang, Q. Mei, Interface allocation precisely customized Janus upconversion nanomotor for atherosclerosis amelioration, Adv. Funct. Mater. 34 (41) (2024) 2405916.

[63] M. Chen, E. Ma, Y. Xing, H. Xu, L. Chen, Y. Wang, Y. Zhang, J. Li, H. Wang, S. Zheng, Dual-modal lateral flow test strip assisted by near-infrared-powered nanomotors for direct quantitative detection of circulating MicroRNA biomarkers from serum, ACS Sens. 8 (2) (2023) 757–766.

[64] M. Liu, L. Chen, Z. Zhao, M. Liu, T. Zhao, Y. Ma, Q. Zhou, Y.S. Ibrahim, A. A. Elzatahry, X. Li, D. Zhao, Enzyme-based mesoporous nanomotors with near-infrared optical brakes, J. Am. Chem. Soc. 144 (9) (2022) 3892–3901.

[65] K. Chen, X. Peng, M. Dang, J. Tao, J. Ma, Z. Li, L. Zheng, X. Su, L. Wang, Z. Teng, General thermodynamic-controlled coating method to prepare janus mesoporous nanomotors for improving tumor penetration, ACS Appl. Mater. Interfaces 13 (43) (2021) 51297–51311.

[66] J. Shao, M. Xuan, H. Zhang, X. Lin, Z. Wu, Q. He, Chemotaxis-guided hybrid neutrophil micromotors for targeted drug transport, Angew. Chem. Int. Ed. Engl. 56 (42) (2017) 12935–12939.

[67] H. Liu, J. Zhang, Y. Jia, X. Liu, X. Chen, W. Zhao, C. Mao, Theranostic nanomotors for tumor multimode imaging and photothermal/photodynamic synergistic therapy, Chem. Eng. J. 442 (2022) 135994.

[68] S. Chen, X. Sun, M. Fu, X. Liu, S. Pang, Y. You, X. Liu, Y. Wang, X. Yan, X. Ma, Dual-source powered nanomotor with integrated functions for cancer photo-theranostics, Biomaterials 288 (2022) 121744.

[69] Z. Chen, T. Xia, Z. Zhang, S. Xie, T. Wang, X. Li, Enzyme-powered Janus nanomotors launched from intratumoral depots to address drug delivery barriers, Chem. Eng. J. 375 (2019) 122109.

[70] M. Qiao, Y. Xing, L. Xie, B. Kong, F. Kleitz, X. Li, X. Du, Temperature-regulated core swelling and asymmetric shrinkage for tunable yolk@shell polydopamine@mesoporous silica nanostructures, Small 18 (52) (2022) e2205576.

[71] Z. Ye, Y. Wang, S. Liu, D. Xu, W. Wang, X. Ma, Construction of nanomotors with replaceable engines by supramolecular machine-based host-guest assembly and disassembly, J. Am. Chem. Soc. 143 (37) (2021) 15063–15072.

[72] D. Xu, C. Zhou, C. Zhan, Y. Wang, Y. You, X. Pan, J. Jiao, R. Zhang, Z. Dong, W. Wang, X. Ma, Enzymatic micromotors as a mobile photosensitizer platform for highly efficient on-chip targeted antibacteria photodynamic therapy, Adv. Funct. Mater. 29 (17) (2019) 1807727.

[73] X. Ma, S. Jang, M.N. Popescu, W.E. Uspal, A. Miguel-López, K. Hahn, D.P. Kim, S. Sánchez, Reversed Janus micro/nanomotors with internal chemical engine, ACS Nano 10 (9) (2016) 8751–8759.

[74] T. Patino, A. Porchetta, A. Jannasch, A. Lladó, T. Stumpp, E. Schäffer, F. Ricci, S. Sánchez, Self-sensing enzyme-powered micromotors equipped with pH-responsive DNA nanoswitches, Nano Lett. 19 (6) (2019) 3440–3447.

[75] X. Ma, A. Jannasch, U.R. Albrecht, K. Hahn, A. Miguel-López, E. Schäffer, S. Sánchez, Enzyme-powered hollow mesoporous janus nanomotors, Nano Lett. 15 (10) (2015) 7043–7050.

[76] M. Wan, Q. Wang, R. Wang, R. Wu, T. Li, D. Fang, Y. Huang, Y. Yu, L. Fang, X. Wang, Y. Zhang, Z. Miao, B. Zhao, F. Wang, C. Mao, Q. Jiang, X. Xu, D. Shi, Platelet-derived porous nanomotor for thrombus therapy, Sci. Adv. 6 (22) (2020) eaaz9014.

[77] X. Arqué, M.D.T. Torres, T. Patiño, A. Boaro, S. Sánchez, C. de la Fuente-Nunez, Autonomous treatment of bacterial infections *in vivo* using antimicrobial micro- and nanomotors, ACS Nano 16 (5) (2022) 7547–7558.
[78] D. Vilela, N. Blanco-Cabra, A. Eguskiza, A.C. Hortelao, E. Torrents, S. Sanchez, Drug-free enzyme-based bactericidal nanomotors against pathogenic bacteria, ACS Appl. Mater. Interfaces 13 (13) (2021) 14964–14973.
[79] A.C. Hortelão, T. Patiño, A. Perez-Jiménez, À. Blanco, S. Sánchez, Enzyme-powered nanobots enhance anticancer drug delivery, Adv. Funct. Mater. 28 (25) (2018) 1705086.
[80] W. Wang, R. Fu, R. Gao, L. Luo, Z. Wang, Y. Xue, J. Sun, M. Pan, M. Hong, L. Qiao, W. Qiao, Q. Mei, J. Wu, Y. Wang, Y. Zhong, J. Liu, F. Tong, H(2)S-powered nanomotors for active therapy of tumors by inducing ferroptosis and lactate-pyruvate axis disorders, ACS Biomater. Sci. Eng. 10 (6) (2024) 3994–4008.
[81] Y.H. Li, S. Zhou, X. Jian, X. Zhang, Y.Y. Song, Asymmetrically coating Pt nanoparticles on magnetic silica nanospheres for target cell capture and therapy, Microchim. Acta 188 (11) (2021) 361.
[82] Y. Xing, S. Tang, X. Du, T. Xu, X. Zhang, Near-infrared light-driven yolk@shell carbon@silica nanomotors for fuel-free triglyceride degradation, Nano Res. 14 (3) (2021) 654–659.
[83] A. Llopis-Lorente, A. García-Fernández, N. Murillo-Cremaes, A.C. Hortelão, T. Patiño, R. Villalonga, F. Sancenón, R. Martínez-Máñez, S. Sánchez, Enzyme-powered gated mesoporous silica nanomotors for on-command intracellular payload delivery, ACS. Nano 13 (10) (2019) 12171–12183.
[84] Z. Cong, S. Tang, L. Xie, M. Yang, Y. Li, D. Lu, J. Li, Q. Yang, Q. Chen, Z. Zhang, X. Zhang, S. Wu, Magnetic-powered Janus cell robots loaded with oncolytic Adenovirus for active and targeted virotherapy of bladder cancer, Adv. Mater. 34 (26) (2022) 2201042.
[85] Z. Zhang, D. Zhang, B. Qiu, W. Cao, Y. Liu, Q. Liu, X. Li, Icebreaker-inspired Janus nanomotors to combat barriers in the delivery of chemotherapeutic agents, Nanoscale 13 (13) (2021) 6545–6557.
[86] B. Mayol, S. Pradana-López, A. García, C. de la Torre, P. Díez, A. Villalonga, C. Anillo, D. Vilela, A. Sánchez, P. Martínez-Ruiz, R. Martínez-Máñez, R. Villalonga, Self-propelled enzyme-controlled IR-mesoporous silica Janus nanomotor for smart delivery, J. Colloid Interface Sci. 671 (2024) 294–302.
[87] J. Wu, S. Yi, Y. Cao, M. Zu, B. Li, W. Yang, M.A. Shahbazi, Y. Wan, R.L. Reis, S. C. Kundu, X. Shi, B. Xiao, Dual-driven nanomotors enable tumor penetration and hypoxia alleviation for calcium overload-photo-immunotherapy against colorectal cancer, Biomaterials 302 (2023) 122332.
[88] X. Chang, M. Zhu, X. Tang, X. Yu, F. Liu, L. Chen, T. Yin, Z. Zhu, Y. Zhang, X. Chen, Enhanced manipulation of tumor microenvironments by nanomotor for synergistic therapy of malignant tumor, Biomaterials 290 (2022) 121853.
[89] M. Xuan, J. Shao, X. Lin, L. Dai, Q. He, Self-propelled Janus mesoporous silica nanomotors with sub-100 nm diameters for drug encapsulation and delivery, Chemphyschem 15 (11) (2014) 2255–2260.
[90] Y. Tao, X. Li, Z. Wu, C. Chen, K. Tan, M. Wan, M. Zhou, C. Mao, Nitric oxide-driven nanomotors with bowl-shaped mesoporous silica for targeted thrombolysis, J. Colloid Interface Sci. 611 (2022) 61–70.
[91] Y. Huang, T. Li, W. Gao, Q. Wang, X. Li, C. Mao, M. Zhou, M. Wan, J. Shen, Platelet-derived nanomotor coated balloon for atherosclerosis combination therapy, J. Mater. Chem. B 8 (26) (2020) 5765–5775.
[92] Q. Wang, Y. Wang, B. Guo, S. Shao, Y. Yu, X. Zhu, M. Wan, B. Zhao, C. Bo, C. Mao, Novel heparin-loaded mesoporous tubular micromotors formed via template-assisted electrochemical deposition, J. Mater. Chem. B 7 (16) (2019) 2688–2695.
[93] X. Bai, W. Peng, Y. Tang, Z. Wang, J. Guo, F. Song, H. Yang, C. Huang, An NIR-propelled janus nanomotor with enhanced ROS-scavenging, immunomodulating and biofilm-eradicating capacity for periodontitis treatment, Bioact. Mater. 41 (2024) 271–292.
[94] A. Loukanov, Light-triggered Janus nanomotor for targeting and photothermal lysis of pathogenic bacteria, Microsc. Res. Tech. 84 (5) (2021) 967–975.
[95] S. Zheng, Y. Wang, S. Pan, E. Ma, S. Jin, M. Jiao, W. Wang, J. Li, K. Xu, H. Wang, Biocompatible nanomotors as active diagnostic imaging agents for enhanced magnetic resonance imaging of tumor tissues *in vivo*, Adv. Funct. Mater. 31 (24) (2021) 2100936.
[96] J. Ye, Q. Fu, L. Liu, L. Chen, X. Zhang, Q. Li, Z. Li, L. Su, R. Zhu, J. Song, H. Yang, Ultrasound-propelled Janus Au NR-mSiO2 nanomotor for NIR-II photoacoustic imaging guided sonodynamic-gas therapy of large tumors, Sci. China Chem. 64 (12) (2021) 2218–2229.
[97] X. Ma, S. Sanchez, A bio-catalytically driven Janus mesoporous silica cluster motor with magnetic guidance, Chem. Commun. 51 (25) (2015) 5467–5470.
[98] X. Ma, S. Sánchez, Bio-catalytic mesoporous Janus nano-motors powered by catalase enzyme, Tetrahedron 73 (33) (2017) 4883–4886.
[99] W. Ban, J. Qu, L. Cai, J. Fu, W. Wu, H. Song, C. Yu, J. Tang, Lipase-powered asymmetric silica nanomotors with a tailored head-tail structure for enhanced mucus penetration, Appl. Mater. Today 34 (2023) 101916.
[100] R. Mestre, N. Cadefau, A.C. Hortelão, J. Grzelak, M. Gich, A. Roig, S. Sánchez, Nanorods based on mesoporous silica containing iron oxide nanoparticles as catalytic nanomotors: study of motion dynamics, ChemNanoMat 7 (2) (2021) 134–140.
[101] X. Jiao, Z. Wang, J. Xiu, W. Dai, L. Zhao, T. Xu, X. Du, Y. Wen, X. Zhang, NIR powered Janus nanocarrier for deep tumor penetration, Appl. Mater. Today 18 (2020) 100504.
[102] C. Fiedler, C. Ulbricht, T. Truglas, D. Wielend, M. Bednorz, H. Groiss, O. Brüggemann, I. Teasdale, Y. Salinas, Reversible speed regulation of self-propelled janus micromotors via thermoresponsive bottle-brush polymers, Chemistry 27 (10) (2021) 3262–3267.
[103] Y.S. Wang, H. Xia, C. Lv, L. Wang, W.F. Dong, J. Feng, H.B. Sun, Self-propelled micromotors based on Au–mesoporous silica nanorods, Nanoscale 7 (28) (2015) 11951–11955.